CD4+ T cell calibration of antigen-presenting cells optimizes antiviral CD8+ T cell immunity

Elise Gressier [1,16] ✉, Jonas Schulte-Schrepping [2,3,16], Lev Petrov[4], Sophia Brumhard[5], Paula Stubbemann[5], Anna Hiller[5], Benedikt Obermayer [6], Jasper Spitzer [7], Tomislav Kostevc[4], Paul G. Whitney[1], Annabell Bachem[1], Alexandru Odainic [1,7], Carolien van de Sandt [1], Thi H. O. Nguyen [1], Thomas Ashhurst [8], Kayla Wilson [1], Clare V. L. Oates[1], Linden. J. Gearing [9,10], Tina Meischel [1], Katharina Hochheiser[1], Marie Greyer[1], Michele Clarke[1], Maike Kreutzenbeck[7], Sarah S. Gabriel [1], Wolfgang Kastenmüller [11], Christian Kurts[12], Sarah L. Londrigan [1], Axel Kallies [1], Katherine Kedzierska [1], Paul J. Hertzog[9,10], Eicke Latz [7], Yu-Chen E. Chen[13], Kristen J. Radford [13], Michael Chopin[14], Jan Schroeder[1], Florian Kurth [5], Thomas Gebhardt [1], Leif E. Sander [5], Birgit Sawitzki[4], Joachim L. Schultze[2,3,15], Susanne V. Schmidt[7,17] & Sammy Bedoui [1,12,17] ✉

Antiviral CD8+ T cell immunity depends on the integration of various contextual cues, but how antigen-presenting cells (APCs) consolidate these signals for decoding by T cells remains unclear. Here, we describe gradual interferon-α/interferon-β (IFNα/β)-induced transcriptional adaptations that endow APCs with the capacity to rapidly activate the transcriptional regulators p65, IRF1 and FOS after CD4+ T cell-mediated CD40 stimulation. While these responses operate through broadly used signaling components, they induce a unique set of co-stimulatory molecules and soluble mediators that cannot be elicited by IFNα/β or CD40 alone. These responses are critical for the acquisition of antiviral CD8+ T cell effector function, and their activity in APCs from individuals infected with severe acute respiratory syndrome coronavirus 2 correlates with milder disease. These observations uncover a sequential integration process whereby APCs rely on CD4+ T cells to select the innate circuits that guide antiviral CD8+ T cell responses.

Antigen-presenting cells (APCs) depend on capturing and presenting viral antigens through major histocompatibility complex (MHC) molecules to prime naive T cells and restimulate antigen-experienced T cells during virus infections[1–3]. Effective T cell responses also hinge on a variety of non-antigenic signals that are relayed from APCs to T cells by co-stimulatory molecules and soluble mediators. It is well established that such contextual cues broadly reflect the exposure of APCs to inflammatory cytokines, such as interferon-α/interferon-β (IFNα/β) and danger signals that stimulate the NF-κB pathway[3,4]. Yet, the number of co-stimulatory molecules and soluble mediators that APCs use to convey these cues to T cells is discrete, and the expression of many of these factors continues to change as the APCs interact with T cells. For example, CD4+ T cells responding to antigen rapidly increase the expression of CD40L and provide stimulation back to the APC via CD40 and the NF-κB pathway[5]. Such 'T cell help' involves cooperation with innate stimuli[6,7], but how APCs integrate these different signals at the cellular level and whether such cooperation requires prolonged interactions with CD4+ T cells or follows more dynamic patterns is currently unclear. Resolving how APCs integrate and relay these different signals to CD8+ T cells is important for our general understanding of how the innate–adaptive cross-talk regulates T cell responses and will provide key insights required to improve CD8+ T cell responses during infection and vaccination.

Here, we systematically dissected how APCs integrate stimulation through IFNα/β and CD40 from CD4+ T cells. We identified an iterative process whereby APCs require IFNα/β-dependent rewiring of the signaling cascade downstream of CD40 that enables the subsequent partition of NF-κB-, IRF1- and FOS-dependent genes into distinct patterns of co-stimulatory molecule expression and mediator provision. This carefully sequenced integration process is critical for antiviral CD8+ T cell responses in a mouse virus infection model, and its activity in APCs from individuals infected with severe acute respiratory syndrome coronavirus 2 (SARS-CoV-2) correlates with CD8+ T cell responses and milder forms of coronavirus disease 2019 (COVID-19).

Results

IFNα/β and CD40 induce distinct responses by dendritic cells

To dissect how APCs integrate signals from IFNα/β and CD40 stimulation, we initially focused on type 1 conventional dendritic cells (cDC1s), known platforms for T cell help[8,9]. We exposed bone marrow-derived CD24hiCD11blo cDC1s (hereafter, BMDC1s) to IFNαA and an antibody that mimics T cell help by cross-linking CD40[6]. RNA sequencing (RNA-seq) revealed that CD40 induced some changes in BMDC1s, but this response was limited compared to >1,000 differentially expressed (false discovery rate (FDR) > 0.05, 1.5-fold change) genes induced by IFNαA (Fig. 1a and Supplementary Table 1). Most IFN-stimulated genes (ISGs)[10] remained unaffected by additional CD40 stimulation (Fig. 1a, 'CD40-unresponsive genes'). However, a subgroup of genes, which included *Ccl4* and *Il15*, was further increased when IFNαA and CD40 antibody were applied together (Fig. 1a, 'amplified genes'). We also observed genes that could not be induced by either stimulus alone but were strongly increased in BMDC1s exposed to both IFNαA and CD40 antibody (Fig. 1a, 'combinatorial genes'). This response included *Ccl5* and *Tnf* and other genes with known roles in the interplay between APCs and T cells, such as *Cd83* and *Cxcl16* (Fig. 1a). We validated these distinct response patterns in separate experiments, focusing on interleukin-15 (IL-15) and CCL4 as examples for the amplified response and tumor necrosis factor-alpha (TNF-α) and CCL5 for the combinatorial synergy between IFNαA and CD40 stimulation (Fig. 1b,c and Extended Data Fig. 1a). Comparable responses could also be elicited when CD40 synergized with IFNβ (Extended Data Fig. 1b) or other innate stimuli, such as polyinosinic–polycytidylic acid (poly(I:C)), lipopolysaccharide (LPS) or cytosine–phosphate–guanine (CpG), which triggered Toll-like receptor 3 (TLR3), TLR4 and TLR9, respectively (Extended Data Fig. 1c). These findings indicate that CD40 synergizes with various innate stimuli in inducing 'amplified' and 'combinatorial' responses in BMDC1s.

cDC1s require in vivo stimulation from both IFNα/β and CD4+ T cells through CD40 to 'amplify' their capacity to provide IL-15 to herpes simplex virus (HSV)-specific CD8+ T cells[6]. To investigate whether priming of HSV-specific CD8+ T cells requires mediators that can only be induced by the synergy between IFNα/β and CD40 (such as CXCL16 and CCL5), we transferred *Cxcr6+/+* and *Cxcr6−/−* bone marrow cells into irradiated hosts and infected them 6–8 weeks later with HSV-1 on the skin. Seven days later, splenic HSV-specific *Cxcr6−/−* CD8+ T cells produced less IFNγ in response to ex vivo antigen restimulation than their *Cxcr6+/+* counterparts (Fig. 1d). CCL5-competent transgenic HSV-specific CD8+ T cells transferred into *Ccl5−/−* mice also had a significant, albeit more subtle, defect in IFNγ production in response to ex vivo antigen restimulation compared to wild-type recipients of HSV-specific transgenic CD8+ T cells (Fig. 1e), indicating that multiple genes required stimulation through both IFNα/β and CD40 for optimal helper-dependent DC–CD8+ T cell interactions in vivo.

IFNα/β change transcription downstream of CD40

Next, we tested whether IFNα/β and CD40 antibody acted concurrently or in sequence. To first investigate whether CD40 stimulation conditioned a more efficient response of BMDC1s to IFNα/β, we stimulated BMDC1s with CD40 antibody for 4 h and added IFNαA for the last 15, 30, 60, 120 or 180 min of the stimulation. *Il15* expression increased after 1–2 h of IFNαA stimulation, and this expression increased more than twofold in the presence of CD40 antibody (Fig. 2a). *Tnf*, *Cxcl16* and *Cd83* were also induced in BMDC1s after 2–3 h of IFNαA stimulation (Fig. 2a), indicating that BMDC1s required ~2 h of IFNα/β exposure before they responded to CD40 triggering. We then determined whether IFNα/β conditioned the BMDC1s for CD40 responses by exposing BMDC1s to IFNα/β over 4 h and adding CD40 antibody for the last 15, 30, 60, 120 or 180 min. *Tnf*, *Cxcl16* and *Cd83* increased after 30–60 min (Fig. 2a), which showed that BMDC1s responded rapidly to CD40 stimulation if exposed to IFNα/β for ~2 h and suggested that BMDC1 need to be exposed to IFNα/β prior to CD40 stimulation IFNα/β conditions the dendritic cells (DCs) to become receptive to T cell help. We also tested this requirement in vivo using HSV-1 skin infection[6]. CD8+ cDC1s residing in the brachial lymph nodes of wild-type mice increased MHC class II expression 2 days after infection, but this increase was absent in *Ifnar2−/−* mice (Extended Data Fig. 1d). Because lack of CD4+ T cells does not impact MHC class II expression by CD8+ cDC1s in the brachial lymph nodes of wild-type mice infected 2 days earlier with HSV-1 on the skin[6], these findings indicate that IFNα/β signals also need to precede CD40-mediated T cell help in vivo.

Next, we tested whether IFNα/β prepared DCs for T cell help by increasing CD40 expression[7]. IFNαA-stimulated and unstimulated BMDC1s increased the expression of CD40 over time similarly (Extended Data Fig. 1e), indicating that surface CD40 expression was not rate limiting in these responses. To investigate whether the 'amplified' and 'combinatorial' responses resulted from the effect of IFNα/β on the pathways downstream of CD40, we performed RNA-seq of BMDC1s stimulated with IFNαA for 4 h (BMDC1-IFN-αA) and compared gene expression to BMDC1s additionally stimulated with CD40 antibody for the last 15 min (BMDC1-IFNαA + CD40-15min) or 30 min (BMDC1-IFNαA + CD40-30min) or over the entire 4-h period (BMDC1-IFNαA + CD40-4h). Overall, BMDC1s changed expression of 341 genes over the 15-min, 30-min and 4-h time points compared to BMDC1-IFNαA, BMDC1-CD40 or unstimulated BMDC1s (Fig. 2b). Unsupervised self-organizing maps (SOMs) of these 341 genes identified smaller groups of genes appearing transiently at 15 min and 30 min (that is, *Ifi44*, *Ifit3* and *Fos*), while different and larger sets of genes clustered at 4 h (that is, *Cd83*, *Il15*, *Cxcl16*, *Il27* and *Cd80*) (Fig. 2c and Supplementary Table 2). General cellular processes, such as 'enhanced survival' and 'increased mRNA stability', were enriched in BMDC1-IFNαA + CD40-30min, while more specific responses, including 'regulation of cytokine production', characterized BMDC1-IFNαA + CD40-4h (Fig. 2d). We also performed coexpression analysis[11] to identify similarly expressed groups of genes ('modules') independently of fold change cutoffs used to define differentially expressed genes across all time points (Fig. 2e and Supplementary Table 3). Genes in modules 1 and 3, such as *Cxcl16* and *Tnf*, responded to the combination of IFNαA and CD40 antibody at 30 min and 4 h (Extended Data Fig. 2a). Modules 2 and 4 grouped genes that were induced by IFNαA (that is, *Oasl1*, *Isg20* and *Il2rg*) or CD40 antibody (that is, *Cxcr4*, *Apol7c* and *Il12b*), respectively, while modules 5 and 6 contained genes with little responsiveness to either stimulation (that is, *Itga3*, *Sox4* and *Irak1*) (Fig. 2e). These modules also differed in GO term enrichments (Fig. 2d). Together, these analyses indicate that IFNα/β changed how BMDC1s responded at the transcriptional level to CD40 stimulation.

IFNαA enable CD40 to activate p65, FOS and IRF1

Next, transcription factor binding motif prediction analysis of the 'amplified' genes suggested the involvement of overlapping transcriptional regulators, including members of the IRF and STAT families (Fig. 3a). More specifically, BMDC1-IFNαA + CD40-30min and BMDC1-IFNαA + CD40-4h were enriched for binding sites for NF-κB, including NFKB1, REL, RELA (p65 subunit) and RELB (Fig. 3a). To test these predictions, we examined canonical and non-canonical NF-κB
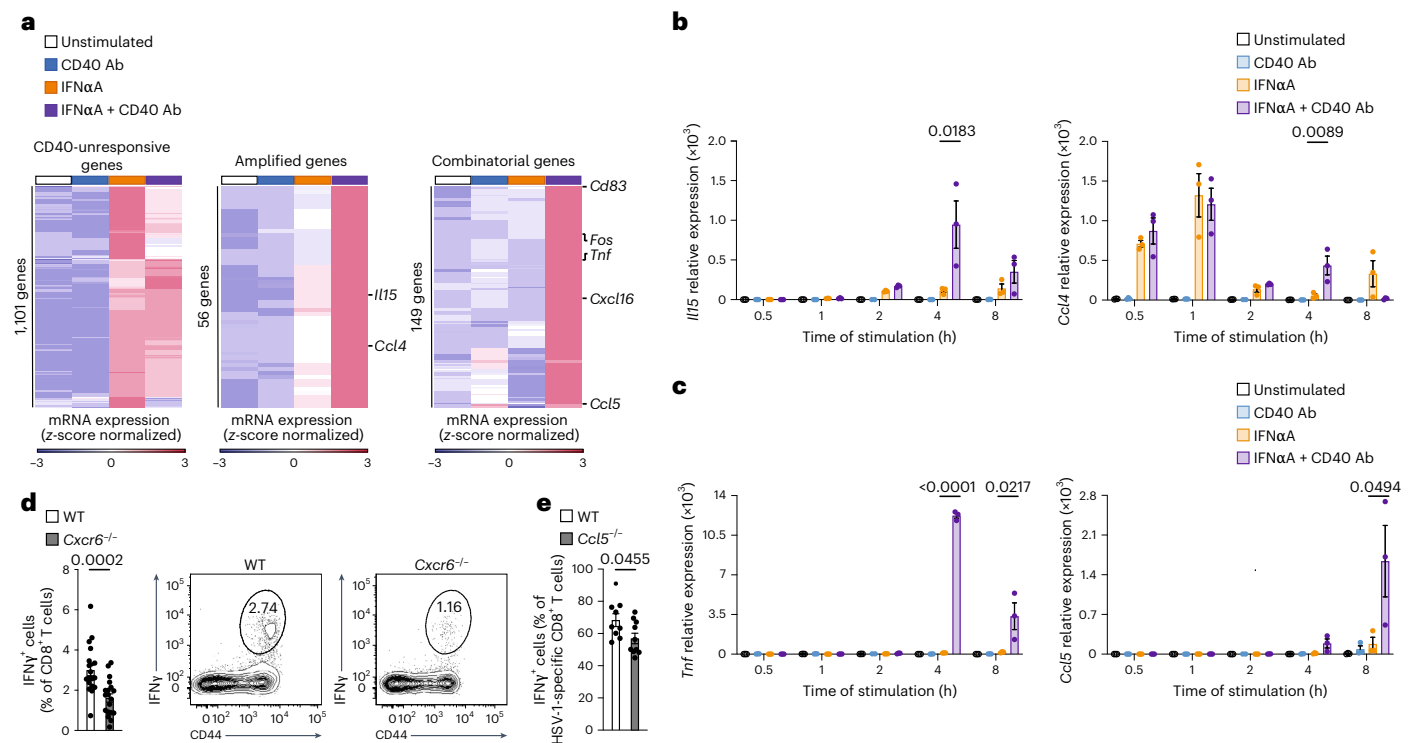
Fig. 1 | IFNα/β and CD40 induce distinct and combinatorial responses in cDC1s. a, Changes in gene expression of BMDC1s stimulated for 4 h with IFNαA (*n* = 6 independent experiments), CD40 antibody (Ab) (*n* = 3 independent experiments) or IFNαA + CD40 antibody (*n* = 3 independent experiments) compared to unstimulated BMDC1s (*n* = 6 independent experiments). Differentially expressed genes are displayed as heat maps after *z*-score transformation of counts per million (CPM). Statistical differences were assessed by one-way analysis of variance (ANOVA); FDR-adjusted *P* ≤ 0.05 and fold change greater than 1.5. **b,c**, Relative expression of *Il15* and *Ccl4* (**b**) and *Tnf* and *Ccl5* (**c**) over time in BMDC1s stimulated with IFNαA and/or CD40 antibody. Data are mean ± s.e.m. from two to three independent experiments. Statistically significant differences between conditions were assessed by one-way ANOVA;

adjusted *P* values are indicated. **d**, IFNγ production after ex vivo antigen restimulation for 5 h by splenic wild-type (WT) and *Cxcr6*^{−/−} HSV-1-specific CD8^{+} T cells 10 days after HSV-1 skin infection of wild-type mice that were irradiated and reconstituted with an equal mix of *Cxcr6*^{−/−} and wild-type bone marrow cells 6–8 weeks earlier. Data are mean ± s.e.m. from three independent experiments (*n* ≥ 5 per experiment). **e**, IFNγ production after ex vivo antigen restimulation for 5 h by transgenic HSV-1-specific CD8^{+} T cells (gBT-I cells) transferred as naive gBT-I cells into wild-type or *Ccl5*^{−/−} mice 1 day before HSV-1 infection and isolated from the spleen 7 days after infection. Data are mean ± s.e.m. from three independent experiments (*n* ≥ 1 per experiment). Statistical significance between conditions in **d** and **e** was assessed by two-tailed Wilcoxon rank-sum test, and respective *P* values are indicated.

signaling cascades in the interplay between IFNαA and CD40 antibody. The induction of amplified genes (*Il15* and *Ccl4*) and combinatorial genes (*Tnf* and *Cxcl16*) in BMDC1-IFNαA + CD40-4h was similar between *Nfkb2*^{−/−} and wild-type BMDC1s (data not shown), indicating that the non-canonical NF-κB pathway was not required. BMDC1-IFNαA + CD40-15min resulted in IκBα degradation and p65 phosphorylation (Fig. 3b and Extended Data Fig. 2c), and the NF-κB inhibitor ammonium pyrrolidinedithiocarbamate (PDTC)[12] impaired the increased expression of *Tnf* and *Ccl4* in BMDC1-IFNαA + CD40-4h (Fig. 3c). These findings highlight that IFNα/β conditioning enabled CD40 to trigger the canonical NF-κB pathway in BMDC1s.

The transcriptional regulator FOS was induced in BMDC1-IFNαA + CD40-15min compared to in BMDC1-IFNαA, BMDC1-CD40 and BMDC1-IFNαA + CD40-4h (Fig. 3d and Supplementary Table 2). We therefore deleted FOS from FLT3L-propagated BMDCs using CRISPR–Cas9 and stimulated these cells for 4 h with IFNαA and CD40 antibody. Compared to non-targeting guide control (NTC) BMDCs, *Il15ra* and *Il27*, but not *Cxcl16* or *Nfkb2*, were reduced in the absence of FOS (Fig. 3e). ERK[13] and CD40 signaling[14] can activate FOS, and we found phosphorylated p38 and ERK in BMDC1-IFNαA + CD40-15min (Fig. 3f). Inhibition of ERK by nimbolide prevented the increase in *Ccl4* expression and partially reduced *Tnf* expression in BMDC1-IFNαA + CD40-4h compared to in BMDC1-IFNαA (Fig. 3c). Together, these findings indicate that

IFNα/β conditioning enables CD40 to activate FOS, likely through activation of ERK and p38.

The 'combinatorial' genes induced by IFNα/β and CD40 antibody were enriched in IRF1 binding sites (Fig. 3g), and expression of *Irf1* was increased in BMDC1-IFNαA + CD40-30min and BMDC1-IFNαA + CD40-4h compared to in BMDC1-IFNαA (Fig. 3h). IRF1 binding signals were enriched in combinatorial genes in BMDC1-IFNαA + CD40-4h compared to in BMDC1-NS, BMDC1-IFNαA and BMDC1-CD40, as revealed by cleavage under targets and tagmentation (CUT&TAG) analysis (Fig. 3i). Endogenous IRF1 was bound to the promoter region of *Cxcl16* in BMDC1-IFNαA + CD40-4h but not in BMDC1-IFNαA, BMDC1-CD40 or BMDC1-NS (Fig. 3j). Moreover, *Irf1*^{−/−} BMDC1s did not induce the expression of *Cxcl16* in response to 4 h of combined IFNα/β and CD40 antibody stimulation (Fig. 3k), and transcription factor binding motifs in the vicinity of IRF1 binding sites were enriched for motifs recognized by p65 (Fig. 3l). Together, these findings show that IFNα/β conditioning enhances the capacity of cDC1s to degrade IκBα and phosphorylate p65, p38 and ERK downstream of CD40, thus enabling CD4^{+} T cells to induce p65-, IRF1- and FOS-dependent transcriptional programs.

Mild COVID-19 is associated with IFNα/β and CD40 synergy

Imbalances in IFNα/β provision[15] and low-avidity CD4^{+} T cell responses[16] are associated with severe COVID-19 (refs. [17,18]), while milder outcomes correlate with virus-specific CD8^{+} T cells[18] and the ability of individuals
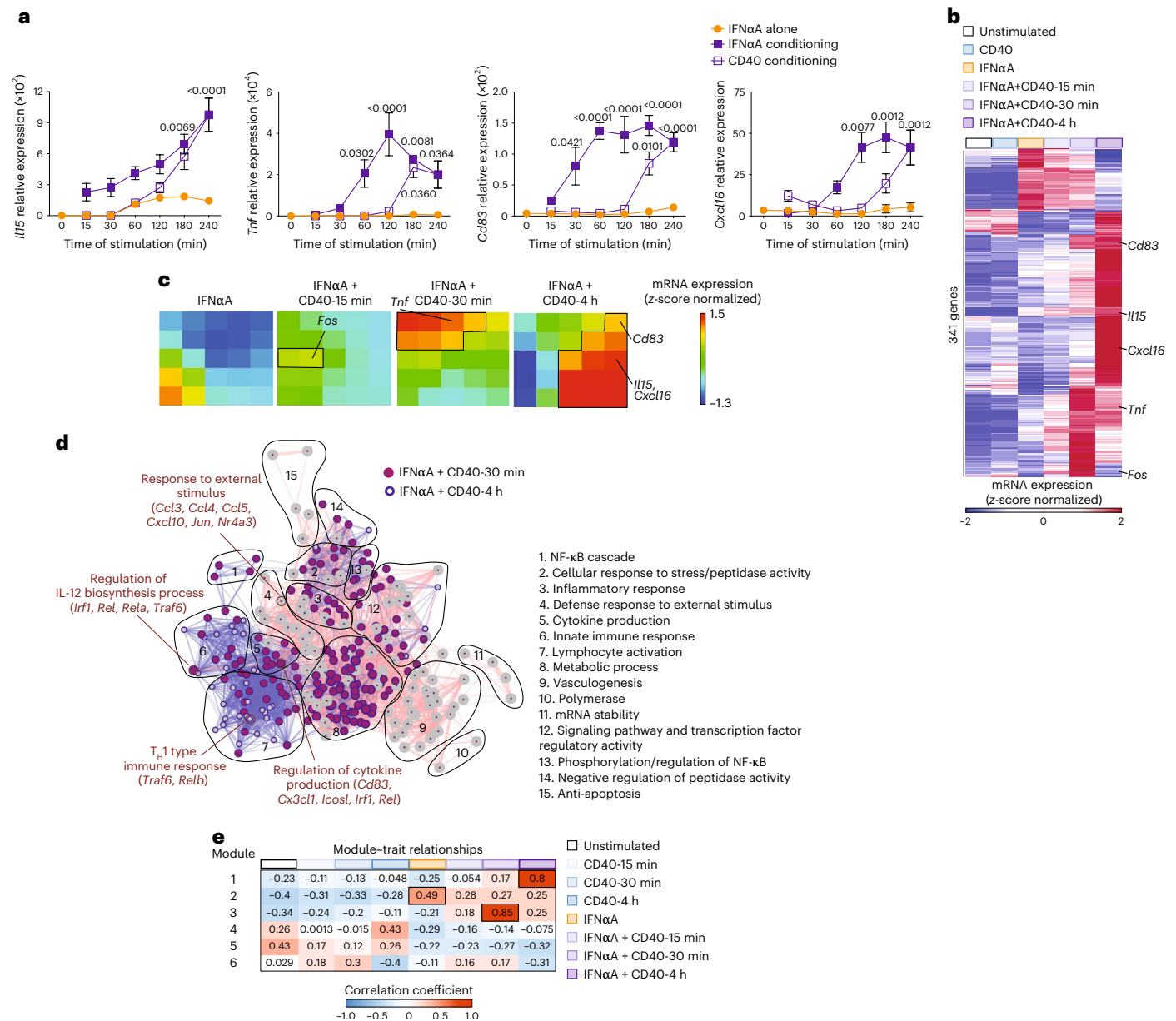
Fig. 2 | IFNα/β conditions cDC1s to enhance transcription in response to CD40 stimulation. a, Changes in the expression of *Il15*, *Tnf*, *Cd83* and *Cxcl16* in BMDC1s stimulated with IFNαA for 4 h and stimulated additionally with CD40 antibody for the last 15, 30, 60, 120, 180 and 240 min ('IFNαA conditioning') or with CD40 antibody for 4 h and stimulated additionally with IFNαA for the last 15, 30, 60, 120, 180 and 240 min ('CD40 conditioning') compared to BMDC1s exposed to IFNαA alone (at least three independent experiments for each time point). Error bars represent mean ± s.e.m. Statistically significant differences between the corresponding conditions and IFNαA at 4 h alone were assessed by one-way ANOVA. **b,c**, Heat map (**b**) and SOM (**c**) of differentially expressed genes between BMDC1s left unstimulated or stimulated with IFNαA alone (IFNαA; *n* = 6 independent experiments) or with IFNαA for 4 h + CD40 for 15 min (IFNαA + CD40-15min; *n* = 3 independent experiments), 30 min (IFNαA + CD40-30min; *n* = 3 independent experiments) or 4 h (IFNαA + CD40-4h; *n* = 3 independent experiments). The 341 genes were clustered into 25 SOM clusters that follow similar patterns of expression with the identification of

select genes in their respective clusters. **d**, Gene Ontology (GO) terms enriched in IFNαA + CD40-30min SOM clusters (clusters 1–4 and 6–8, as in panel **c**) and IFNαA + CD40-4h SOM clusters (clusters 5, 9, 10, 13–15, 18–20 and 23–25, as in panel **c**). Nodes represent the GO term, edges represent a score inversely proportional to the genes shared between the two GO terms, and the size of the nodes is proportional to the enrichment score. GO terms with a *P* value of ≤0.005 that relate to three or more GO terms are displayed; T$_H$1, type 1 helper T cell. **e**, Correlation coefficients of weighted gene correlation network analysis (WGCNA) eigengenes combining transcriptional results from RNA-seq of BMDC1s that were unstimulated (*n* = 6 independent experiments) or stimulated with CD40 for 15 min (CD40-15min; *n* = 3 independent experiments), CD40 for 30 min (CD40-30min; *n* = 3 independent experiments), CD40 for 4 h (CD40-4h; *n* = 3 independent experiments), IFNαA alone for 4 h (IFNαA; *n* = 6 independent experiments), IFNαA for 4h + CD40 for 15 min (IFNαA + CD40-15min), IFNαA for 4 h + CD40 for 30 min (IFNαA + CD40-30min) or IFNαA for 4 h + CD40 for 4 h (IFNαA + CD40-4h; *n* = 3 independent experiments).

to respond to CCL5 (ref. 19) and CXCL16 (ref. 20). To investigate the synergy between IFNα/β and CD40 during SARS-CoV-2 infection, we isolated CD14⁻HLA-DR⁺ DCs from the blood of individuals with COVID-19 4 to 35 days after symptom onset[21]. This included mild to moderate

disease (WHO (World Health Organization) score of 2–5) and severe disease (WHO score of 6–8) (Supplementary Table 7). CD14⁻HLA-DR⁺ DCs from individuals with severe disease had significantly reduced expression of MHC class II (HLA-DR) compared to CD14⁻HLA-DR⁺ DCs from
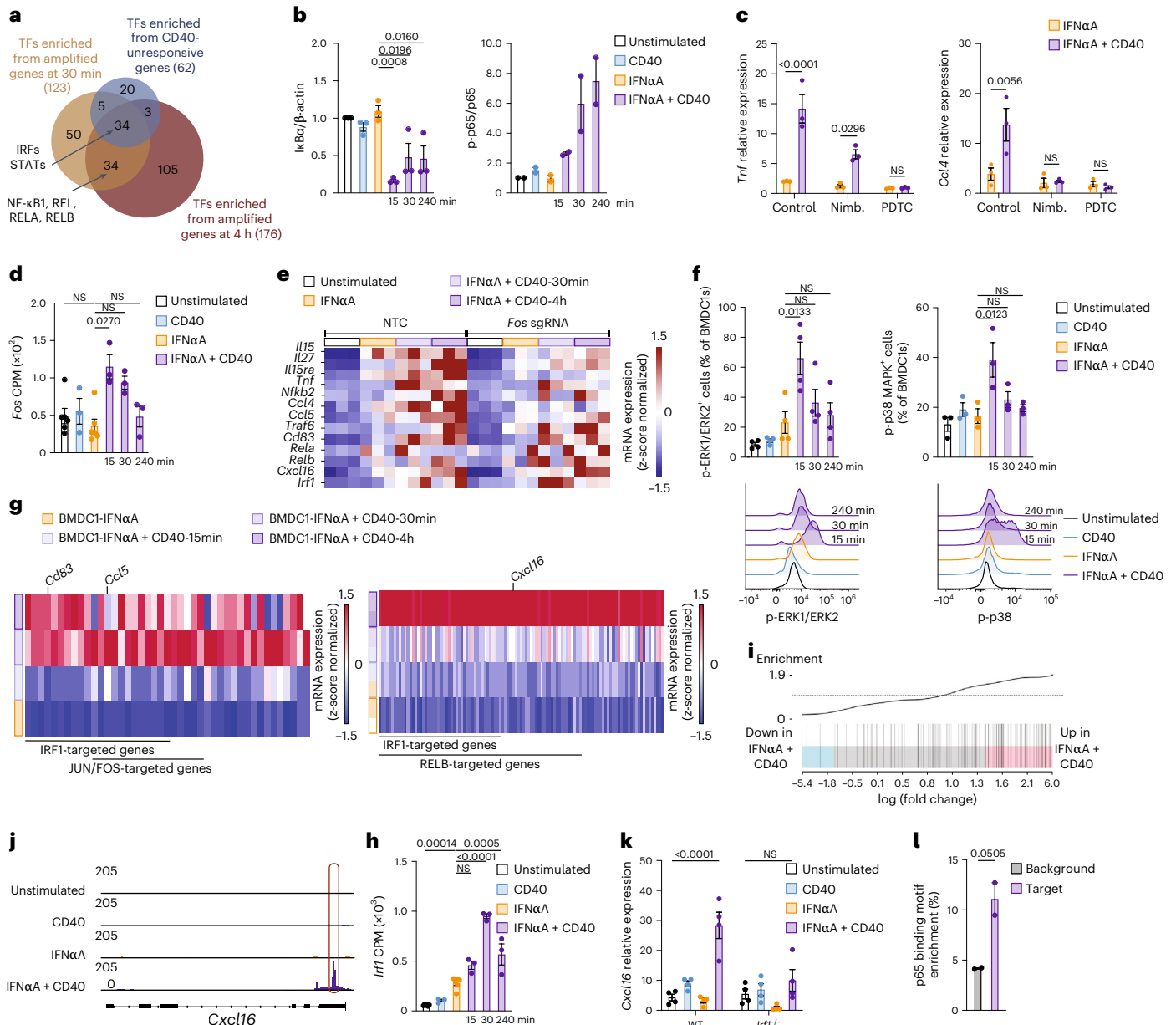
Fig. 3 | IFNαA conditioning enables CD40 to activate a network of transcription factors that includes p65, IRF1 and FOS. a, Transcription factor (TF) motifs enriched for 'CD40-unresponsive genes' and 'amplified genes' at 30 min and 4 h (as in Fig. 2b) and displayed as Venn diagrams. **b**, IκBα degradation ($n = 3$ independent experiments) and p65 phosphorylation ($n = 2$ independent experiments) in BMDC1s, as in Fig. 2b. **c**, *Tnf* and *Ccl4* expression in BMDC1s stimulated as in Fig. 2b in the absence or presence of inhibitors for ERK (nimbolide) and the NF-κB pathway (PDTC). Data are displayed relative to treatment alone and are pooled from three independent experiments. Error bars represent mean ± s.e.m. Adjusted *P* values of the statistically significant differences as assessed by two-way ANOVA are indicated; Nimb, nimbolide; NS, not significant. **d**, *Fos* expression based on RNA-seq of BMDC1s, stimulated as Fig. 2b, expressed as CPM. **e**, Relative expression of select genes (*Il15*, *Il27*, *Il15ra*, *Tnf*, *Nfkb2*, *Ccl4*, *Ccl5*, *Traf6*, *Cd83*, *Rela*, *Relb*, *Cxcl16* and *Irf1*) in BMDC1s transduced with *Fos* single guide RNA (sgRNA) or NTC and stimulated as in Fig. 2b ($n = 3$ independent experiments). **f**, Phosphorylation of ERK1/ERK2

(p-ERK1/ERK2) and p38 MAPK (p-p38 MAPK) ($n = 3–4$ independent experiments) in BMDC1s as in Fig. 2b. Pooled data and representative histograms are displayed. **g**, Expression of 'combinatorial genes' in BMDC1s as in Fig. 2b. **h**, Expression of *Irf1* in RNA-seq data from BMDC1s stimulated as in Fig. 2b, expressed as CPM. **i**, Enrichment of IRF1 binding signals in combinatorial genes in BMDC1-IFN-αA + CD40-4h ($P < 0.0001$; $n = 2$ replicates). **j**, IRF1 binding signals analyzed using CUT&Tag in BMDC1s stimulated as in Fig. 2b ($n = 2$ replicates). **k**, Expression of *Cxcl16* in wild-type or *Irf1*−/− BMDC1s stimulated as in Fig. 2b. Data are mean ± s.e.m. from three independent experiments. Adjusted *P* values were assessed by two-way ANOVA. **l**, p65 binding motif enrichment in DNA bound to IRF1 in BMDC1s as in Fig. 2b, expressed as target relative to the entire genomic background data. Statistical testing was performed using the cumulative binomial distribution to compare target binding to background signal. Data are mean ± s.e.m. from two replicates. Error bars in **b**, **d**, **f** and **h** represent mean ± s.e.m. Adjusted *P* values of the statistically significant differences between the corresponding conditions as assessed by one-way ANOVA are indicated.

individuals with mild disease (Fig. 4a). A similar pattern was observed in CD14⁺CD11c⁺ monocytes, with a significant reduction in MHC class II expression compared to that observed in mild COVID-19 cases (Fig. 4a).

To test whether IFNα/β signals contribute to MHC class II expression, we collected blood samples 4 to 35 days after symptom onset from individuals with COVID-19 who had developed neutralizing antibodies

against type I IFN (IFN-AAB)[22]. CD14^{−}HLA-DR^{+} DCs and CD14^{+}CD11c^{+} monocytes from IFN-AAB^{+} individuals had an even stronger reduction of MHC class II than observed in those from individuals with mild disease (Fig. 4a). The expression of CD40 on CD14^{−}HLA-DR^{+} DCs in individuals with severe disease increased irrespective of IFN-AAB but was reduced in CD14^{+}CD11c^{+} monocytes in individuals with IFN-AAB (Fig. 4a), suggesting that IFNα/β regulate the ability of DCs and monocytes to receive T cell help through the expression of MHC class II[5,23,24].

Next, we used published single-cell RNA-seq (scRNA-seq) data from individuals with COVID-19 (ref. 25) to examine the expression of the 'CD40-unresponsive', 'amplified' and 'combinatorial' gene signatures identified above. This included peripheral blood mononuclear cells (PBMCs) from individuals with COVID-19 (mild, WHO score of 3, $n = 16$; moderate, WHO score of 4–5, $n = 11$; severe, WHO score of 7, $n = 23$) collected within the first 25 days after symptom onset before availability of vaccination. These were compared to samples from healthy or otherwise hospitalized individuals who tested negative for SARS-CoV-2, were serologically negative or had no indication of acute COVID-19 disease based on clinical or laboratory parameters (HC; $n = 13$)[25]. We analyzed 31,736 classical monocytes and 722 myeloid DCs using reference-based cell-type annotation and clustering (Methods), referred to here as CD14^{+} monocytes and CD1C^{+} DCs, respectively. CD14^{+} monocytes from individuals with mild disease[25] were significantly enriched for the 'amplified' and 'combinatorial' responses (that is, *CD83*, *CXCL16*, *NFKB2* and *JUND*) compared to CD14^{+} monocytes from individuals with moderate or severe disease or from healthy control individuals (Fig. 4b,c and Supplementary Table 5). Also, CD1C^{+} DCs from individuals with mild COVID-19 had increased transcription of genes of the 'amplified' and 'combinatorial' responses, such as *CD83*, *EGR1* and *REL*, compared to CD1C^{+} DCs from individuals with severe COVID-19, which in turn had increased expression of CD40-unresponsive genes, such as *IFIT3*, *MX1* and *IRF7* (Fig. 4d and Supplementary Table 6). Similar patterns were observed in scRNA-seq data of a second cohort[26], which included three individuals with moderate disease (respiratory symptoms and pneumonia), four individuals with severe disease (supplemental oxygen requirement) collected 2–16 days after symptom onset and five asymptomatic healthy control individuals from whom samples were collected before the widespread circulation of SARS-CoV-2 (Extended Data Fig. 3a).

We also performed scRNA-seq on PBMC samples from the COVID-19 cohort above, which included IFN-AAB^{+} individuals[22]

(Supplementary Table 7). CD14^{+} monocytes from IFN-AAB^{+} individuals had lower induction of prototypical ISGs, such as *ISG15* and *IFIT2*, than CD14^{+} monocytes from healthy individuals and individuals with disease without IFN-AAB (Extended Data Fig. 3b). Furthermore, the expression of *HLA-DRA*, *HLA-DRB1*, *TNF*, *CD83* and *CCL4* was reduced in CD14^{+} monocytes from individuals with severe COVID-19 and in IFN-AAB^{+} individuals compared to in healthy individuals and in individuals with COVID-19 without IFN-AAB (Extended Data Fig. 3b). To gain more robust insights into data distribution, we integrated our data with comparable published scRNA-seq data sets[21,27,28], including a study examining four IFN-AAB^{+} individuals[28]. This yielded 179,012 single-cell CD14^{+} monocyte transcriptomes across 263 samples (HC, $n = 39$; WHO score of 1–3, mild, $n = 79$; WHO score of 4–5, moderate, $n = 82$; WHO score of 6–8, severe, $n = 52$; WHO score of 7–8, severe + IFN-AAB, $n = 11$). *HLA-DRB1*, *CD83* and *TNF* were significantly reduced in individuals with COVID-19 with increasing disease severity, reaching a minimum in individuals with IFN-AAB (Extended Data Fig. 3b). Furthermore, the 'amplified' and 'combinatorial' signatures were reduced in CD14^{+} monocytes from individuals with severe COVID-19, with and without IFN-AAB, compared to in CD14^{+} monocytes from individuals with mild disease (Extended Data Fig. 3c). Together, these findings indicate that IFNα/β signals are critical drivers of 'amplified' and 'combinatorial' responses during SARS-CoV-2 infection.

Reanalysis of published single-cell assay for transposase-accessible chromatin with sequencing (scATAC-seq) data sets[29] from PBMCs of individuals with COVID-19 indicated that CD14^{+} monocytes from individuals with mild disease had significantly increased accessibility of more than 300 genes, including *IL15*, *CD83*, *TNF* and *CXCL16*, compared to CD14^{+} monocytes from individuals with moderate and severe COVID-19 (Fig. 4e,f). Furthermore, Hallmark enrichment analysis of more accessible genes in CD14^{+} monocytes from individuals with mild COVID-19 compared to CD14^{+} monocytes from healthy control individuals identified 'IFNγ response' and 'TNF signaling via NF-κB' as major pathways differentially regulated in mild COVID-19 (Fig. 4g). To investigate whether these responses can be elicited in vitro in human cDC1s, we differentiated human CD141^{+}CADM1^{+}CLEC9A^{+} cDC1s (hDC1s) from blood-derived CD34^{+} stem cells using FLT3L, stem cell factor and IL-4 (ref. 30) and stimulated them with human recombinant IFNα and human CD40 Ab separately or in combination for 18 h. hDC1s

---

**Fig. 4 | Combinatorial responses to IFNα/β and CD40 antibody by DCs and monocytes correlate with milder outcomes of COVID-19. a**, HLA-DR expression of CD14^{+}CD11c^{+} monocytes and CD14^{−}HLA-DR^{+} DCs from individuals with COVID-19 with mild or moderate symptoms (WHO score of 2–5; $n = 11$) or severe disease with (WHO score of 6–8; $n = 3–6$) and without ($n = 10$) IFN-AAB. Data are displayed as box and whisker plots showing the median and the 25th and 75th percentiles and two whiskers at 1.5× the interquartile range (IQR) of the mean fluorescence intensity (MFI) and percentage of CD40^{+} cells. **b**, Single-sample gene set variation analysis (GSVA) of the 'CD40-unresponsive', 'amplified' and 'combinatorial' gene signatures in scRNA-seq data from CD14^{+} monocytes and CD1C^{+} DCs from PBMCs of individuals with mild (WHO score of 3; $n = 16$), moderate (WHO score of 4–5; $n = 11$) or severe (WHO score of 7; $n = 23$) COVID-19 and healthy control (HC) individuals ($n = 13$; reanalyzed from ref. 25). Box plots as in panel **a**. Data points are colored and shaped according to disease severity and stage based on days after onset of symptoms, respectively. Wilcoxon rank-sum test P values are shown. **c**, Gene set enrichment analysis plots (top) showing enrichment curves of the 'amplified' and 'combinatorial' signatures in the differentially expressed genes (two-sided Wilcoxon rank-sum test, minimum percentage = 0.1, $\log_2$(fold change) > 0.2) in CD14^{+} monocytes from mild compared to severe COVID-19 cases as in **b**. The $\log_{10}$(FDR P values) and the $\log_2$(fold change) values of the differentially expressed genes are shown as a volcano plot (bottom). Genes are colored according to the 'CD40-unresponsive', 'amplified' or 'combinatorial' signature; P_{adj}, adjusted P value.

d, Differential expression of 'CD40-unresponsive', 'amplified' and 'combinatorial' signature genes in CD1C^{+} DCs from healthy control individuals and individuals with mild, moderate and severe cases of COVID-19, as in **a**, determined using a two-sided Wilcoxon rank-sum test. **e**, Heat map showing GeneScores for disease-specific, significantly differentially accessible genes in scATAC-seq data of CD14^{+} monocytes from PBMC samples derived from individuals with mild (WHO score of 1–3; $n = 7$ samples), moderate (WHO score of 4–5; $n = 4$) or severe (WHO score of 6–7; $n = 6$) COVID-19 and healthy control individuals ($n = 6$; reanalyzed from ref. 29) determined using a two-sided Wilcoxon rank-sum test (FDR ≤ 0.01 and $\log_2$ (fold change) ≥ 0.58). **f**, Imputed GeneScores of *IL15*, *CD83*, *CXCL16* and *TNF* in CD14^{+} monocytes grouped according to COVID-19 severity as in **e**. Data are displayed as violin plots with overlaying box and whisker plots showing the median and 25th and 75th percentiles and two whiskers at 1.5× IQR. **g**, Differentially accessible genes (FDR ≤ 0.01 and $\log_2$(fold change) ≥ 0.58) in CD14^{+} monocytes from individuals with mild COVID-19 compared to healthy control individuals, as in **e**, visualized as a volcano plot showing $−\log_{10}$(FDR) and $\log_2$(fold change) values (left) and the corresponding enriched Hallmark terms for the 789 genes with increased accessibility in mild COVID-19 CD14^{+} monocytes compared to healthy control monocytes displayed as dot plots showing gene counts and adjusted P values per term (right). **h**, Secretion of TNF in hDC1s stimulated with IFNα and/or CD40 antibody for 18 h. Data are mean ± s.e.m. from six donors. Statistical significance for differences between conditions was assessed by one-way ANOVA, and adjusted P values are indicated.

secreted TNF in response to IFNα when aided by CD40 triggering, but not after treatment with IFNα alone (Fig. 4h). These observations indicated that APCs from individuals with mild, but not severe, COVID-19 had increased chromatin accessibility and transcription of genes requiring the synergy between IFNα/β and CD40 described in the mouse experiments.
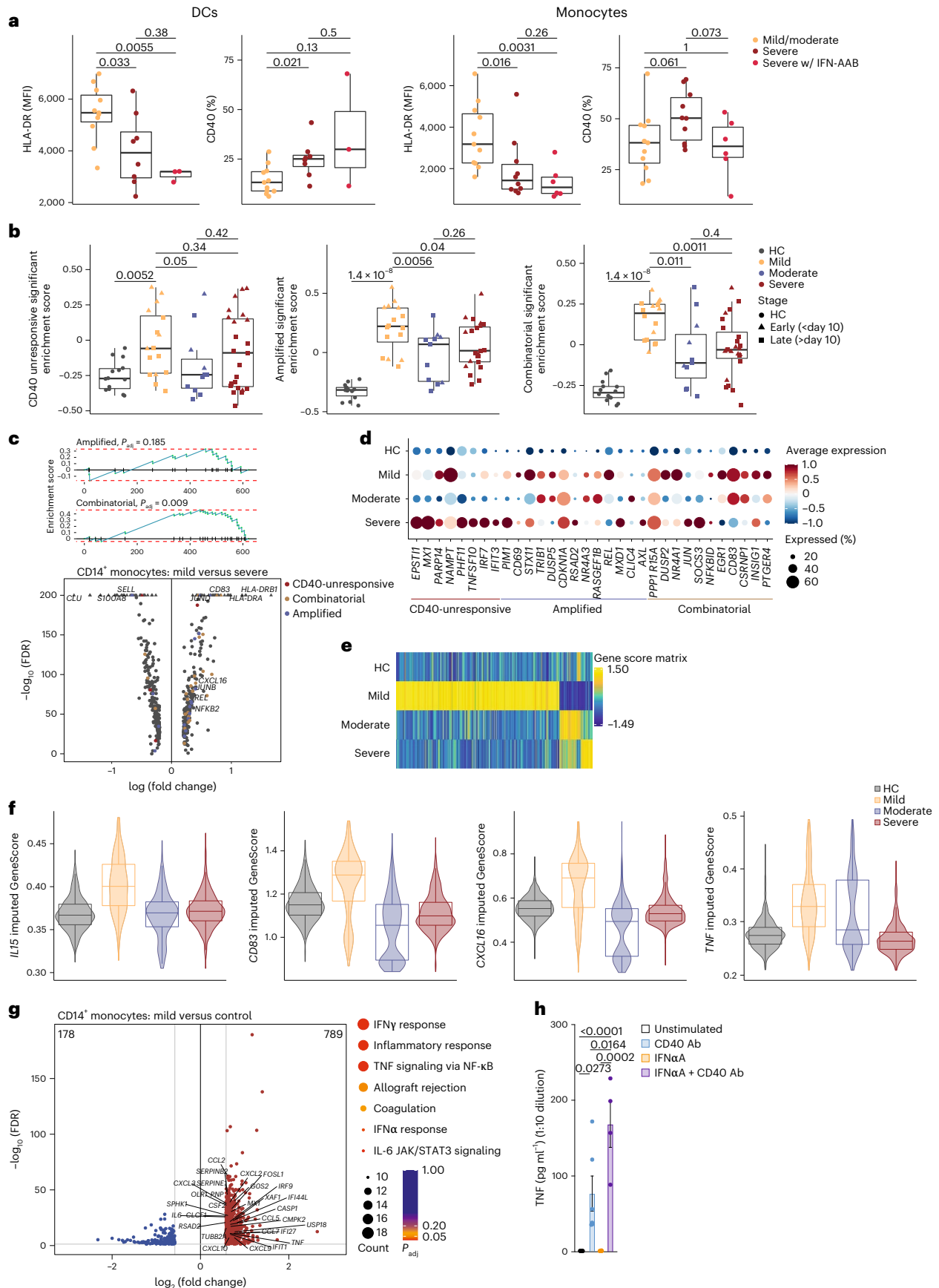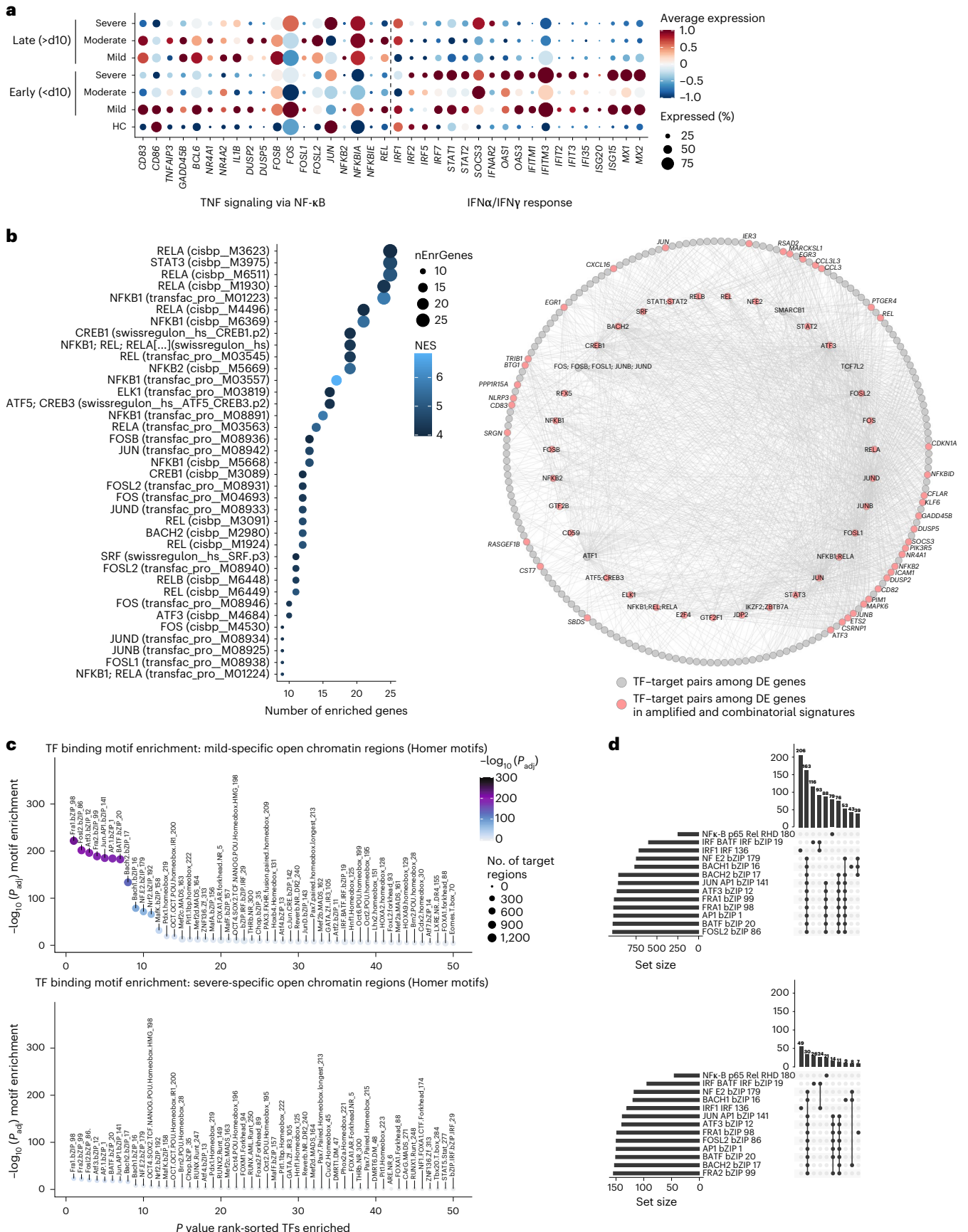
Fig. 5 | Enrichment of NF-κB- and FOS-dependent transcriptional responses in APCs from individuals with mild, but not severe, COVID-19. a, Differentially expressed genes between disease severities and stages in CD14⁺ monocytes representing the significantly enriched Hallmark terms 'IFNγ response', 'IFNα response' and 'TNF signaling via NF-κB', displayed as dot plots. **b,** RcisTarget transcription factor binding motif enrichment based on differentially expressed genes (two-tailed Wilcoxon rank-sum test, minimum percentage = 0.1, log₂(fold change) > 0.2) in CD14⁺ monocytes from individuals with mild compared to severe COVID-19, as in Fig. 4a. Data are visualized as a dot plot (left) showing the number of enriched genes and the normalized enrichment score per motif. The inner circle (right) shows the enriched transcription factors for all differentially expressed (DE) genes, and the outer circle shows the respective target genes responsible

for their enrichments. Transcription factors enriched for the genes overlapping with the 'amplified' and 'combinatorial' gene signatures and the target genes are colored in red. NES, normalized enrichment score. **c,** Transcription factor binding motif enrichment based on significantly differentially accessible peaks in CD14⁺ monocytes from individuals with mild or severe COVID-19 compared to CD14⁺ monocytes from healthy control individuals. Data are based on scATAC-seq data[29] and are displayed as dot plots showing FDR-adjusted *P* values of the enrichments and the number of target regions per transcription factor binding motif. **d,** Target regions of the top 10 highest enriched transcription factor binding motifs and motifs corresponding to IRF1 and p65 (RELA), shown as UpSet plots comparing the number of target regions.

CD40 triggers NF-κB and FOS-dependent transcription in mild COVID-19

To explore whether IFNα/β also affected the signaling cascade downstream of CD40 in human APCs, we subjected the differentially expressed genes that were significantly higher in CD14⁺ monocytes from individuals with mild COVID-19 than in CD14⁺ monocytes from individuals with severe COVID-19 to enrichment analyses using the Hallmark database[31] and transcription factor binding motifs[32]. There was a significant enrichment of genes associated with the NF-κB pathway, including *CD83*, *CD86*, *TNFAIP3*, *IL1B*, *DUSP2*, *NFKB2* and *REL* (Fig. 5a and Supplementary Table 5). We also observed preferential involvement of the NF-κB family (NFKB1, RELA and RELB) and the FOS and JUN families (AP-1; Fig. 5b). Visualization of the links between predicted transcription factors and their target genes within the differentially expressed genes between mild and severe COVID-19 indicated a dense regulatory network controlled by NF-κB, FOS and JUN transcription factors (Fig. 5b).

Similarly, transcription factor binding motif enrichment analyses in differentially accessible chromatin regions of CD14⁺ monocytes from individuals with mild or severe COVID-19 compared to those from healthy control individuals[29] predicted members of the FOS family as key regulators (Fig. 5c). The enrichment score and number of accessible target regions of the predicted transcription factors, including FRA1/FRA2, FOSL2 and JUN, were higher in CD14⁺ monocytes from individuals with mild COVID-19 than in CD14⁺ monocytes from individuals with severe COVID-19 (Fig. 5c,d). Furthermore, the top 10 predicted transcription factor binding motifs and motifs corresponding to IRF1 and p65 (RELA) revealed large and distinct sets of target regions for the identified key regulator families among more accessible chromatin regions in CD14⁺ monocytes from mild COVID-19 cases than those from healthy control individuals. There were also substantially lower numbers of target regions with increased accessibility in CD14⁺ monocytes from individuals with severe COVID-19 than in CD14⁺ monocytes from healthy control individuals (Fig. 5d). These findings suggest that the

amplified and combinatorial responses enriched in CD14⁺ monocytes in individuals with mild COVID-19 are regulated by signal integration through transcription factors of the NF-κB, FOS and JUN families.

Mild COVID-19 is associated with 'helped' CD8⁺ T cells

To test whether IFNα/β-dependent provision of T cell help to DCs and monocytes affects the CD8⁺ T cell response, we used the PBMC scRNA-seq data set from the cohort of individuals with COVID-19 and healthy control individuals defined above (Fig. 4b). We analyzed 11,734 CD8⁺ T cells using reference-based cell-type annotation and clustering (Methods) and compared their transcriptional profiles to published gene signatures that reflected CD8⁺ T cell priming in the presence ('helped') or absence ('unhelped') of CD4⁺ T cell help for DCs[33]. CD8⁺ T cells from individuals with moderate and severe COVID-19 were enriched for 'unhelped' profiles (including *CD200*, *CD200R1*, *BTLA*, *ID3* and *PDCD1*) compared to CD8⁺ T cells from individuals with mild COVID-19 (Fig. 6a,b). Clustering analysis further indicated that individuals with mild and moderate COVID-19 were enriched in CD8⁺ T cell subsets with transcriptional profiles (*IL7R*, *TCF7*, *JUNB* and *JUND*) indicative of early effector or activated memory T cells[34,35] (Fig. 6c,d and Supplementary Table 8, cluster 3). CD8⁺ T cells with characteristics of terminal differentiation (*CX3CR1* and *ISG15*, cluster 5) also dominated in individuals with severe COVID-19 (Fig. 6c,d) and had a reduction in 'helped' signatures (that is, *CD69*, *IL2RA* and *TNF*) and a corresponding gain in the 'unhelped' signature (that is, *IL6R*, *CD9*, *ISG15* and *PDCD1*) (Fig. 6e). We found comparable patterns in published scRNA-seq data from two other cohorts of individuals with COVID-19 (Extended Data Fig. 4a–c)[36,37]. We used cytometry by time of flight (CyTOF) to examine protein expression in CD8⁺ T cells from blood samples of 9 healthy control individuals and individuals with COVID-19 with mild (WHO score of 2–3; *n* = 25) or severe (WHO score of 7–8; *n* = 18) disease and IFN-AAB⁺ individuals with severe disease (WHO score of 7–8; *n* = 9)[21] collected 4 to 30 days after symptom onset (Supplementary Table 7). Dimensionality reduction using uniform manifold approximation and

Fig. 6 | Severe outcomes of COVID-19 are associated with 'unhelped' CD8⁺ T cells. a, UMAP visualization of scRNA-seq profiles of 11,734 CD8⁺ T cells from individuals with mild (WHO score of 3; *n* = 16), moderate (WHO score of 4–5; *n* = 11) or severe (WHO score of 7; *n* = 23) COVID-19 and healthy control individuals (*n* = 13; reanalyzed from ref. 25). Cells are split and colored according to disease severity. **b,** GSVA of 'helped' and 'unhelped' T cell signatures derived from published gene expression[33] profiles of mouse CD8⁺ T cells primed in the presence or absence of CD4⁺ T cells. Data are displayed as box and whisker plots showing the median and 25th and 75th percentiles and two whiskers at 1.5× IQR. Two-sided Wilcoxon rank-sum test *P* values are shown. **c,** UMAP of CD8⁺ T cells segregated into clusters 0–5 (left) and heat map of the respective proportionate cluster occupancy per disease severity (right) as in **a**. **d,** Expression of key genes associated with clusters 0–5 as in **c**. **e,** AUCell enrichment of genes derived from published gene expression[33] profiles of mouse CD8⁺ T cells primed in the presence or absence of CD4⁺ T cells as in **b**, grouped according to the clustering as in **c** and displayed as violin plots of area under the curve (AUC) scores. FDR-

corrected Dunn's multiple comparison test *P* values are indicated. **f,** UMAP visualization of CD8⁺ T cells from whole-blood samples from healthy control individuals (*n* = 10) and individuals with COVID-19 (mild, *n* = 22; severe, *n* = 21; severe with IFN-AAB, *n* = 9) analyzed by CyTOF. The rightmost plot shows the UMAP colored according to FlowSOM clustering, while the four plots on the left show the distribution of events across the groups. **g,** PCA analysis plot showing average PC1 and PC2 values for all the events per individual as in **f**, colored according to the sample group. Ellipses show an estimated region of group accumulation, arrows represent correlation of the respective marker with either of the PC axes, and arrow length represents correlation strength. **h,** Mean scaled signal intensities for KLRG1, CXCR3 and CD69 (left) and LAG3 (right) displayed as box and whisker plots showing the median and 25th and 75th percentiles and two whiskers at 1.5× IQR. **i,** Relative abundance of CD27⁻KLRG1⁺ cells in the total CD8⁺ T cell fraction displayed as box and whisker plots showing the median and the 25th and 75th percentiles and two whiskers at 1.5× IQR. Statistics in **h** and **i** show two-sided Benjamini–Hochberg-corrected pairwise Wilcoxon *P* values.

projection (UMAP) and clustering with the FlowSOM algorithm indicated differences in the composition of CD8^{+} T cells between individuals with COVID-19 with different disease severity (Fig. 6f). Individuals with

mild COVID-19 had increased proportions of CD27^{+}CD8^{+} T cells with memory potential[6] (Fig. 6f and Extended Data Fig. 4d,e, clusters 17, 19 and 21), while individuals with severe COVID-19 had greater proportions
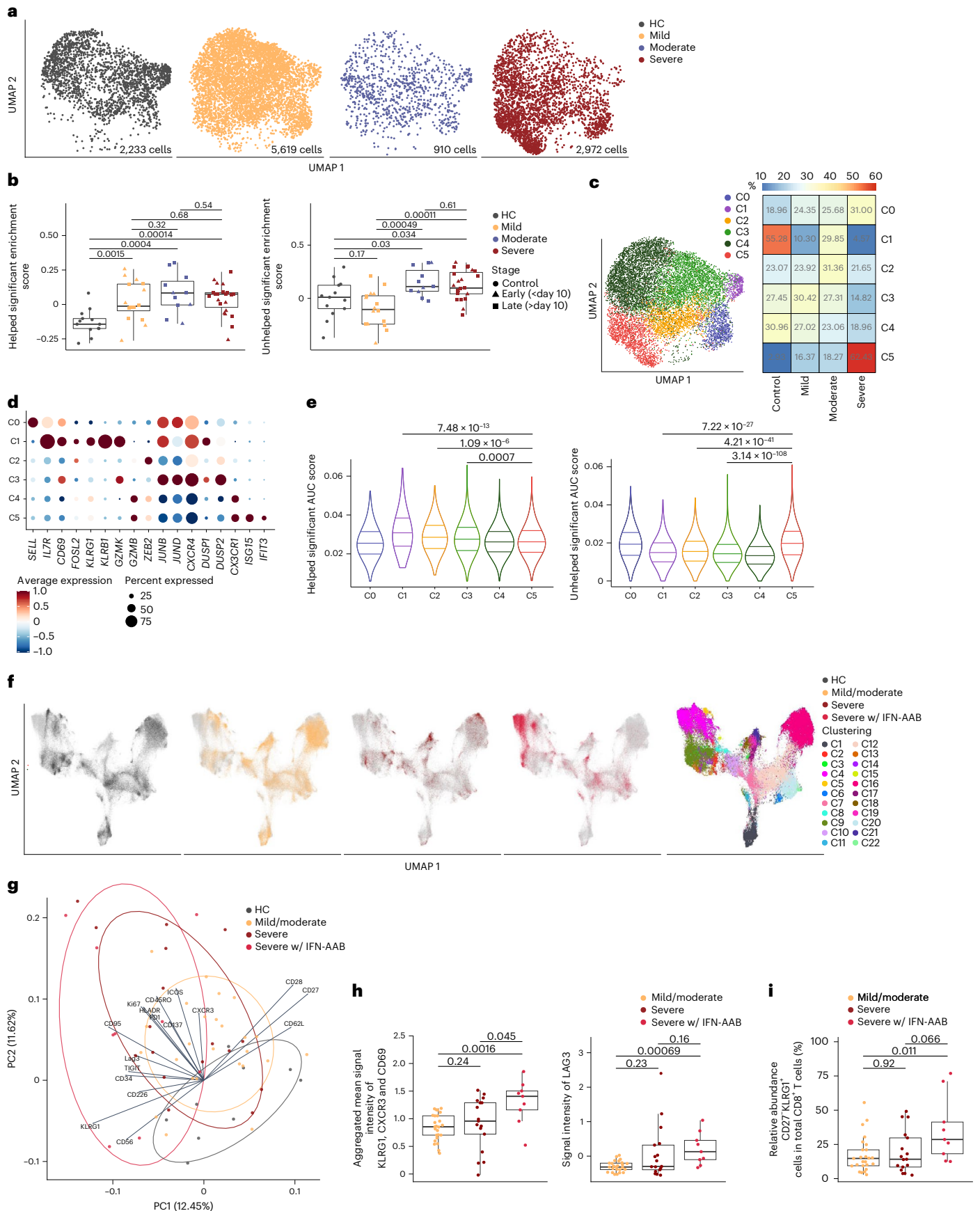
of CD27⁻KLRG1⁺CD8⁺ T cells (clusters 3 and 8) than healthy individuals or individuals with mild disease (Fig. 6f and Extended Data Fig. 4d,e). Principal component analysis (PCA) of CD8⁺ T cells from individuals with mild and severe COVID-19 identified the expression of CD27 and KLRG1 as distinct features of CD8⁺ T cells from individuals with mild and severe disease, respectively (Fig. 6g,i), and CD8⁺ T cells from individuals with severe disease were enriched for LAG3 (Fig. 6h), a molecule induced by priming with unhelped DCs[33]. These findings indicate that severe outcomes of COVID-19 are associated with unhelped phenotypes of CD8⁺ T cells.

Discussion

Our findings uncovered an iterative consolidation process, in which innate stimuli, such as IFNα/β or TLR agonists, determined broad response options in APCs, and CD4⁺ T cells subsequently partitioned these into distinct sets of co-stimulatory molecules, cytokines and chemokines through CD40L. Together, these consecutive signals endowed APCs with optimal capacities to orchestrate effective antiviral CD8⁺ T cell responses in mouse HSV-1 infections and during community-acquired SARS-CoV-2 infections, where effective consolidation of IFNα/β and CD40 signals in APCs correlated with milder outcomes of COVID-19.

The conditioning of APCs by IFNα/β to become receptive to T cell help involved increased expression of MHC class II and distinct changes in how the APCs responded to CD40 stimulation. The changes in CD40 responsiveness were not just a function of increased expression of CD40 alone[8], as spontaneously matured CD40ʰⁱ DCs in mice and CD40ʰⁱ APCs in individuals with severe COVID-19 were unable to engage 'helper'-dependent programs. Instead, the capacity to receive help depended on additional changes in the signaling cascade downstream of CD40. These endowed APCs with the capacity to rapidly engage a network of transcription factors, including p65, IRF1 and FOS, and likely others, such as JUN, to select a distinct group of genes that provide the DCs with optimal capacities to prime CD8⁺ T cells responding to antigen. Some of the transcription factors were directly regulated by IFNα/β and CD40 stimulation, suggesting that conditioning also enhanced the availability of relevant transcription factors. These responses were not exclusive to the cooperation between IFNα/β and CD40, as similar patterns of CD40-dependent calibration also occurred in DCs stimulated through different TLRs. Together with increased chromatin accessibility at binding sites for the above-mentioned transcription factors in promoter regions of key genes regulated through IFNα/β and CD40, our study revealed a multitude of transcriptional and post-translational changes as a functional basis for how innate cues condition APCs to become receptive to T cell help, thus enabling CD4⁺ T cells to calibrate APCs for optimal stimulation of CD8⁺ T cell responses.

We have investigated the relevance of these findings for antiviral CD8⁺ T cell immunity in a mouse model of HSV-1 skin infection and showed that optimal HSV-specific CD8⁺ T cell responses depended on contextual cues that require IFNα/β and NF-κB signal integration by DCs. Notably, we translated these experimental insights to individuals with SARS-CoV-2 infection and demonstrated that the consecutive activation of APCs by IFNα/β and CD4⁺ T cells played an important role in regulating how APCs orchestrate CD8⁺ T cell responses during COVID-19. This interpretation not only helps align a number of currently unlinked findings in COVID-19, such as an association of milder disease with effective provision of CXCL16 (ref. 20) and CCL5 (ref. 19), high-avidity CD4⁺ T cells[16] and effective CD8⁺ T cell responses[18], but also raises the prospect of 'unhelped' APCs launching too many terminally differentiated CD8⁺ T cells that contribute to immunopathology in individuals with severe COVID-19. It is important to acknowledge limitations around our findings in individuals with COVID-19. Our study cannot discern if the observed failures in signal integration by APCs and preponderance of terminally differentiated CD8⁺ T cells are

a 'cause' or 'effect' of severe COVID-19 or are more likely a complex combination of both. Moreover, it is possible that interindividual differences in T cell antigen receptor epitopes, precursor frequencies of antigen-specific CD8⁺ T cells and a great number of many other covariates (that is, age, gender and comorbidities) influence the interaction between APCs and CD8⁺ T cells in individuals with COVID-19. However, having validated our findings across multiple unrelated clinical data sets, it is unlikely that our findings simply represent the confounding effects of any one of these covariates. We likely also missed some of the more nuanced aspects of the interaction between APCs and naive CD8⁺ T cells that take place in lymph nodes before symptom onset, which are difficult to capture as the precise time point of infection is unknown in community-acquired infections, and lymph nodes are not as amenable as blood for routine sampling, especially in individuals with mild disease.

Collectively, our findings demonstrate the reliance of antiviral immunity on a step-wise, carefully orchestrated consolidation process, whereby APCs combine and integrate innate signals and, after selection by CD4⁺ T cells, produce a discrete set of co-stimulatory molecules and soluble mediators that adapt responding CD8⁺ T cells to the specific challenge. In showing how innate and adaptive signals cooperate to partition tailored responses from multiple broad and overlapping innate pathways and demonstrating functional relevance of these processes in mouse and human virus infections, our study provides critical new insights into how the host mounts effective antiviral immunity.

Online content

Any methods, additional references, Nature Portfolio reporting summaries, source data, extended data, supplementary information, acknowledgements, peer review information; details of author contributions and competing interests; and statements of data and code availability are available at https://doi.org/10.1038/s41590-023-01517-x.

References

1. Chow, A., Brown, B. D. & Merad, M. Studying the mononuclear phagocyte system in the molecular age. *Nat. Rev. Immunol.* **11**, 788–798 (2011).
2. Joffre, O. P., Segura, E., Savina, A. & Amigorena, S. Cross-presentation by dendritic cells. *Nat. Rev. Immunol.* **12**, 557–569 (2012).
3. Cabeza-Cabrerizo, M., Cardoso, A., Minutti, C. M., Pereira da Costa, M. & Reis e Sousa, C. Dendritic cells revisited. *Annu. Rev. Immunol.* **39**, 131–166 (2021).
4. Ardouin, L. et al. Broad and largely concordant molecular changes characterize tolerogenic and immunogenic dendritic cell maturation in thymus and periphery. *Immunity* **45**, 305–318 (2016).
5. Borst, J., Ahrends, T., Babala, N., Melief, C. J. M. & Kastenmuller, W. CD4⁺ T cell help in cancer immunology and immunotherapy. *Nat. Rev. Immunol.* **18**, 635–647 (2018).
6. Greyer, M. et al. T cell help amplifies innate signals in CD8⁺ DCs for optimal CD8⁺ T cell priming. *Cell Rep.* **14**, 586–597 (2016).
7. Schulz, O. et al. CD40 triggering of heterodimeric IL-12 p70 production by dendritic cells in vivo requires a microbial priming signal. *Immunity* **13**, 453–462 (2000).
8. Eickhoff, S. et al. Robust anti-viral immunity requires multiple distinct T cell-dendritic cell interactions. *Cell* **162**, 1322–1337 (2015).
9. Hor, J. L. et al. Spatiotemporally distinct interactions with dendritic cell subsets facilitates CD4⁺ and CD8⁺ T cell activation to localized viral infection. *Immunity* **43**, 554–565 (2015).
10. Rusinova, I. et al. Interferome v2.0: an updated database of annotated interferon-regulated genes. *Nucleic Acids Res.* **41**, D1040–D1046 (2013).

11. Yu, X. et al. Isotype switching converts anti-CD40 antagonism to agonism to elicit potent antitumor activity. *Cancer Cell* **37**, 850–866 (2020).

12. Schreck, R., Meier, B., Mannel, D. N., Droge, W. & Baeuerle, P. A. Dithiocarbamates as potent inhibitors of nuclear factor κB activation in intact cells. *J. Exp. Med.* **175**, 1181–1194 (1992).

13. Lavoie, H., Gagnon, J. & Therrien, M. ERK signalling: a master regulator of cell behaviour, life and fate. *Nat. Rev. Mol. Cell Biol.* **21**, 607–632 (2020).

14. Kashiwada, M. et al. Tumor necrosis factor receptor-associated factor 6 (TRAF6) stimulates extracellular signal-regulated kinase (ERK) activity in CD40 signaling along a Ras-independent pathway. *J. Exp. Med.* **187**, 237–244 (1998).

15. Hadjadj, J. et al. Impaired type I interferon activity and inflammatory responses in severe COVID-19 patients. *Science* **369**, 718–724 (2020).

16. Bacher, P. et al. Low-avidity CD4^{+} T cell responses to SARS-CoV-2 in unexposed individuals and humans with severe COVID-19. *Immunity* **53**, 1258–1271 (2020).

17. Schultze, J. L. & Aschenbrenner, A. C. COVID-19 and the human innate immune system. *Cell* **184**, 1671–1692 (2021).

18. Sette, A. & Crotty, S. Adaptive immunity to SARS-CoV-2 and COVID-19. *Cell* **184**, 861–880 (2021).

19. Galani, I. E. et al. Untuned antiviral immunity in COVID-19 revealed by temporal type I/III interferon patterns and flu comparison. *Nat. Immunol.* **22**, 32–40 (2021).

20. Pairo-Castineira, E. et al. Genetic mechanisms of critical illness in COVID-19. *Nature* **591**, 92–98 (2021).

21. Georg, P. et al. Complement activation induces excessive T cell cytotoxicity in severe COVID-19. *Cell* **185**, 493–512 (2022).

22. Akbil, B. et al. Early and rapid identification of COVID-19 patients with neutralizing type I interferon auto-antibodies. *J. Clin. Immunol.* **42**, 1111–1129 (2022).

23. Bedoui, S., Heath, W. R. & Mueller, S. N. CD4^{+} T-cell help amplifies innate signals for primary CD8^{+} T-cell immunity. *Immunol. Rev.* **272**, 52–64 (2016).

24. Wu, R. & Murphy, K. M. DCs at the center of help: origins and evolution of the three-cell-type hypothesis. *J. Exp. Med.* **219**, e20211519 (2022).

25. Schulte-Schrepping, J. et al. Severe COVID-19 is marked by a dysregulated myeloid cell compartment. *Cell* **182**, 1419–1440 (2020).

26. Arunachalam, P. S. et al. Systems biological assessment of immunity to mild versus severe COVID-19 infection in humans. *Science* **369**, 1210–1220 (2020).

27. Su, Y. et al. Multi-omics resolves a sharp disease-state shift between mild and moderate COVID-19. *Cell* **183**, 1479–1495 (2020).

28. van der Wijst, M. G. P. et al. Type I interferon autoantibodies are associated with systemic immune alterations in patients with COVID-19. *Sci. Transl. Med.* **13**, eabh2624 (2021).

29. Wilk, A. J. et al. Multi-omic profiling reveals widespread dysregulation of innate immunity and hematopoiesis in COVID-19. *J. Exp. Med.* **218**, e20210582 (2021).

30. Pearson, F. E. et al. Human CLEC9A antibodies deliver Wilms' tumor 1 (WT1) antigen to CD141^{+} dendritic cells to activate naive and memory WT1-specific CD8^{+} T cells. *Clin. Transl. Immunol.* **9**, e1141 (2020).

31. Liberzon, A. et al. The Molecular Signatures Database (MSigDB) Hallmark gene set collection. *Cell Syst.* **1**, 417–425 (2015).

32. Aibar, S. et al. SCENIC: single-cell regulatory network inference and clustering. *Nat. Methods* **14**, 1083–1086 (2017).

33. Ahrends, T. et al. CD4^{+} T cell help confers a cytotoxic T cell effector program including coinhibitory receptor downregulation and increased tissue invasiveness. *Immunity* **47**, 848–861 (2017).

34. Kaech, S. M. & Wherry, E. J. Heterogeneity and cell-fate decisions in effector and memory CD8^{+} T cell differentiation during viral infection. *Immunity* **27**, 393–405 (2007).

35. Pipkin, M. E. Runx proteins and transcriptional mechanisms that govern memory CD8 T cell development. *Immunol. Rev.* **300**, 100–124 (2021).

36. Bernardes, J. P. et al. Longitudinal multi-omics analyses identify responses of megakaryocytes, erythroid cells, and plasmablasts as hallmarks of severe COVID-19. *Immunity* **53**, 1296–1314 (2020).

37. Chua, R. L. et al. COVID-19 severity correlates with airway epithelium–immune cell interactions identified by single-cell analysis. *Nat. Biotechnol.* **38**, 970–979 (2020).

[1]Department of Microbiology and Immunology at the Doherty Institute for Infection and Immunity, The University of Melbourne, Melbourne, Victoria, Australia. [2]Life and Medical Sciences (LIMES) Institute, University of Bonn, Bonn, Germany. [3]Systems Medicine, Deutsches Zentrum für Neurodegenerative Erkrankungen (DZNE), Bonn, Germany. [4]Translational Immunology, Berlin Institute of Health (BIH) & Charité University Medicine, Berlin, Germany. [5]Infectious Diseases and Respiratory Medicine, Charité, Universitätsmedizin Berlin, Berlin, Germany. [6]Berlin Institute of Health at Charité, Universitätsmedizin Berlin, Core Unit Bioinformatics, Berlin, Germany. [7]Institute of Innate Immunity, University of Bonn, Bonn, Germany. [8]Sydney Cytometry Core Research Facility, Charles Perkins Centre, Centenary Institute and University of Sydney, Sydney, New South Wales, Australia. [9]Centre for Innate Immunity and Infectious Diseases, Hudson Institute of Medical Research, Clayton, Victoria, Australia. [10]Department of Molecular and Translational Science, Monash University, Clayton, Victoria, Australia. [11]Würzburg Institute of Systems Immunology, Max Planck Research Group, Julius-Maximilians-Universität Würzburg, Würzburg, Germany. [12]Institute of Experimental Immunology, University of Bonn, Bonn, Germany. [13]Mater Research Institute, The University of Queensland, Brisbane, Queensland, Australia. [14]Department of Biochemistry, Biomedicine Discovery Institute, Monash University, Clayton, Victoria, Australia. [15]PRECISE Platform for Single Cell Genomics and Epigenomics, DZNE and University of Bonn, Bonn, Germany. [16]These authors contributed equally: Elise Gressier, Jonas Schulte-Schrepping. [17]These authors jointly supervised this work: Susanne V. Schmidt, Sammy Bedoui. ✉e-mail: elise.gressier07@gmail.com; sbedoui@unimelb.edu.au

Methods

Mice

C57BL/6, $Ccl5^{-/-}$, $Cxcr6^{-/-}$, $Ifnar2^{-/-}$, $Irf1^{-/-}$ and CD45.1[+] gBT-I mice were bred and maintained at the animal facility of the Department of Microbiology and Immunology, The University of Melbourne. All animal experiments were approved by The University of Melbourne Animal Ethics Committee.

Human samples

This study includes a subset of individuals enrolled between March 2020 and April 2021 in the Pa-COVID-19 study, a prospective observational cohort study assessing pathophysiology and clinical characteristics of individuals with COVID-19 at Charité Universitätsmedizin, Berlin[38]. The study was approved by the Institutional Review board of Charité (EA2/066/20). Written informed consent was provided by all individuals or legal representatives for participation in the study. Specifics about the participants per application (flow cytometry, CyTOF and scRNA-seq), including COVID-19 status, time point of sampling after onset of symptoms, sex, age and outcome, are listed in Supplementary Table 7 and are described elsewhere[21,22]. Human umbilical cord blood was obtained with written informed consent from the Queensland Cord Blood Bank and approval from the Mater Human Research Ethics Committee (HREC13/MHS/86).

In vitro generation of BMDC1s

Single-cell suspensions from mouse bone marrow were cultured with FLT3L to generate BMDCs[6]. Red blood cells were removed using 1 ml of red blood cell lysis buffer (Sigma-Aldrich) per mouse for 90 s. Cells were cultured at 1.5×10^6 cells per ml in complete medium supplemented with 1.32 mM L-glutamine, 10% fetal calf serum, 90 μM β-mercaptoethanol, 100 U ml^{-1} penicillin, 0.2 g liter^{-1} streptomycin and 150 ng ml^{-1} FLT3L (BioXCell). Following 8 days of culture at 37 °C, cells were stained for 30 min on ice with CD45R/B220 (RA3-6B2), SIRPα (P84), CD11c (N418), CD11b (M1/70), I-A/E (M5114) and CD24 (M1/69) antibodies. cDC1 or CD8^{+} DC equivalents were identified by CD24^{high}SIRPα^{low}CD11b^{low}CD45R/B220^{-} and were sorted using a FACS Aria III (BD Biosciences). Following sorting, BMDC1s were washed and resuspended before stimulation. Stimulation was performed on bulk BMDCs or sorted BMDC1s with IFNα (PBL; 1,000 U ml^{-1}), IFNβ (R&D Systems; 1 μg ml^{-1}), LPS (Sigma-Aldrich; 10 μg ml^{-1}), CpG (1668, GeneWorks; 1.6 nmol ml^{-1}) or poly(I:C) (InvivoGen; 10 μg ml^{-1}) in the presence or absence of monoclonal antibody to CD40 (CD40 Ab; FGK45.5, Miltenyi Biotec; 10 μg ml^{-1}). Cells and supernatants were collected at different time points thereafter. Pharmacological inhibition of NF-κB and ERK pathways was achieved with 1 h pretreatment using PDTC (ab141406, 10 μM) and nimbolide (ab142138, 10 μM), respectively.

Cytokine and chemokine determination

Supernatants were subjected to BD Cytometric Bead Array measurement of CCL4 (limit of detection of 4.88 pg ml^{-1}), CCL5 (limit of detection of 1.22 or 4.88 pg ml^{-1}) and TNF-α (limit of detection of 39.07 or 9.7 pg ml^{-1}), according to the manufacturer's instructions. Samples were assessed using an LSRFortessa and FACS Diva software 6.1.3, and all concentrations were determined relative to a standard curve.

Real-time PCR

Cells were resuspended in TRIzol (Life Technologies), and mRNA was extracted using a Direct-zol RNA MicroPrep kit (Zymo Research) following the manufacturer's instructions. cDNA was synthesized with an Omniscript RT kit for reverse transcription (Qiagen) using oligo(dT) primers (Promega) and RNaseOUT recombinant ribonuclease inhibitor (Thermo Fisher Scientific). Real-time PCR was performed with Taqman Universal PCR master mix (Life Technologies) with primers/probes for 18S (Mm03928990_g1), *B2m* (Mm00437762_m1), *Ccl4* (Mm00443111_m1), *Ccl5* (Mm01302427_m1), *Cd83* (Mm00486868_m1), *Cxcl16*

(Mm00469712_m1), *Gapdh* (Mm99999915_g1), *Hprt* (Mm00446968_m1), *Il15* (Mm00434210_m1), *Il15ra* (Mm04336046_m1), *Il27* (Mm00461162_m1), *Irf1* (Mm01288580_m1), *Nfkb2* (Mm00479807_m1), *Rela* (Mm00501346_m1), *Relb* (Mm00485664_m1), *Tnf* (Mm00443258_m1) and *Traf6* (Mm00493836_m1).

RNA-seq and data analysis

Gene expression changes were investigated using RNA-seq. Up to 100 ng of total RNA was used for library preparation, according to the manufacturer's protocol, and was either sequenced in a 125-base pair (bp) paired-end run on a HiSeq HT sequencer (Illumina) or in a 50-bp single-read QuantSeq 3′-mRNA (Lexogen) run. Reads were aligned against the mouse genome mm10 by STAR v2.5.3a. Gene quantification was performed via the E/M algorithm in PartekFlow (v8.0.19.0707) and normalized as CPM. Genes with a mean expression of ≤1 CPM under all conditions were excluded from further analysis, resulting in 10,222 present genes for ANOVA in the Partek Genomics Suite (PGS, v7.18.0402). Genes with a fold change of 1.5 and an FDR-adjusted *P* value of ≤0.05 were defined as differentially expressed between two tested conditions. GO enrichment for the modules was performed using DAVID[39] with the GOTERM_BP_DIRECT annotation. GO terms were filtered by unadjusted $P \le 0.05$ and visualized using ggplot2. Biological interpretation of differentially expressed genes was performed with the following tools. Gene set enrichment analysis was performed using the GSEA application (v4.0.3) and the Hallmark gene set published by the Broad Institute. Enrichments were plotted using ggplot2 (v3.3.3)[40]. Cytoscape was used to visualize enriched GO terms as a network with the two plugins BiNGO (v3.0.3) and EnrichmentMap (v3.2.1). WordCloud plugin (v3.1.3) was used to visualize the most frequent annotation associated within a cluster of GO terms. All present genes were used as input for a WGCNA, performed using the WGCNA R package (v1.70-3), to identify correlations of gene expression within the data set in an unbiased approach. The β-value was set at 23. For the module dissimilarity, a threshold of 0.42 was chosen, and the minimal cluster size was set to 30 genes. The prediction of transcription factor binding motifs was performed using the Cytoscape plugin iRegulon (v1.3) with a minimum normalized enrichment score of 3 and a maximum FDR on motif similarity of 0.001. All potential transcription factors annotated to the enriched binding motifs were used in the Venn diagram to illustrate their overlaps.

CUT&Tag and analysis

The CUT&Tag experiments were performed as previously described[41] with a hyperactive in situ ChIP library prep kit purchased from Epicypher (CUTANA CUT&Tag Assays) following the manufacturer's recommendations. A minimum of 1×10^5 stimulated BMDC1s were bound to activated concanavalin A-coated magnetic beads and were subjected to immunoprecipitation with 0.5 μg of primary antibody (anti-IRF1, D5E4, Cell Signaling Technology; rabbit anti-mouse IgG control). Immunoprecipitated DNA was amplified with high-fidelity 2× PCR mix (Epicypher) using universal barcodes i5 and uniquely barcoded i7 primers and 21 cycles. PCR products were purified with AMPure XP beads and eluted in water. Libraries were sequenced on an Illumina NextSeq platform, and 150-bp paired-end reads were generated. Fastq reads for each sample were aligned to the mm39 reference genome using bwa (v0.7.17). PCR duplicates were removed using picard tools' MarkDuplicates (v2.25.0), and peaks were called using macs2 (v2.2.7.1) with the '−nomodel' parameter. To establish consensus peaks between all conditions, peak sets were merged using homer's mergePeaks (v4.11.1), and reads in consensus peaks were counted for each replicate using subread's featureCounts (v2.0.0). PCA plots were generated using R (v4.1) and the prcomp function. Differentially occupied peaks were established using the limma package (v3.46.0) and its voom, lmFit and eBayes functions. Motif occupancy at peaks was established with homer and the findMotifsGenome function (v4.11.1).

Immunoblotting

BMDC1s were lysed in resuspension with RIPA buffer containing 50 mM Tris-HCl (pH 8), 150 mM sodium chloride, 1% NP-40, 0.5% sodium deoxycholate and 0.1% SDS (Sigma-Aldrich) supplemented with PhosSTOP phosphatase inhibitor cocktail tablets (Roche) and cOmplete protease inhibitor cocktail tablets (Roche). Cell lysates were rotated at 4 °C for 30 min and clarified at 4 °C at 13,000g for 10 min. Proteins were denatured for 5 min at 90 °C with sample buffer containing 350 mM Tris-HCl (pH 6.8–5), 5% β-mercaptoethanol, 10% SDS, 36% glycerol and 0.0012% bromophenol blue. Proteins were then separated using NuPAGE 4–12% Bis-Tris gels (Thermo Fisher Scientific). Proteins were transferred onto nitrocellulose membranes (Bio-Rad) and blocked for 30 min with either 5% milk or 5% bovine serum albumin (BSA; for phosphorylated proteins) in PBS or TBS (for phosphorylated proteins) with 0.1% Tween 20. The following primary antibodies were used: rabbit anti-NF-κB p65 (D14E12), mouse anti-phospho S536 NF-κB p65 (7F1), rabbit anti-IκBα (44D4) and rabbit anti-β-actin (13E5), all purchased from Cell Signaling Technology. Membranes were incubated with horseradish peroxidase-conjugated secondary antibodies goat anti-rabbit IgG and horse anti-mouse IgG (Cell Signaling Technology) and subsequently with a Novex ECL chemiluminescent substrate reagent kit before imaging. Quantitative analysis of the signal intensity was performed using ImageJ software.

PhosFlow cytometry

Following in vitro stimulation of BMDCs, 100 µl of warm PhosFlow Lyse/Fix Buffer (BD Biosciences) was directly added to the samples and incubated for 10 min at 37 °C. Samples were then resuspended in PhosFlow Perm Buffer III (BD Biosciences) and incubated for 30 min on ice. After being washed twice, samples were stained for 1 h at room temperature with the antibodies described above supplemented with antibody to phospho-P44/42 MAPK (ERK1/ERK2; Thr 202/Tyr 204; 197G2; Cell Signaling Technology) and phospho-p38 MAPK (Thr 180/Tyr 182; 4NIT4KK; Thermo Fisher Scientific). A Biosciences Cytek Aurora was used for the measurement of samples, and FlowJo software (TreeStar) was used for analysis.

CRISPR–Cas9 gene editing

Freshly isolated bone marrow precursors were edited via electroporation before culture with FLT3L, as described previously[42]. In brief, per 10×10^6 mouse bone marrow precursors to be electroporated, 61 pmol of Cas9 nuclease (IDT) and 300 pmol of sgRNA (Synthego) were combined and incubated for 10 min at room temperature, generating Cas9–sgRNA ribonucleoprotein complex. Bone marrow precursors (10×10^6) were then washed with 1× PBS twice and resuspended in 20 µl of P3 buffer (Lonza) combined with the Cas9–sgRNA complex and electroporated using 4D-Nucleofector (Lonza) using the pulse code CM-137. Prewarmed medium was immediately added in electroporation wells to allow cells to recover for 10 min at 37 °C. Cells were subsequently cultured for 8 days in complete medium supplemented with FLT3L, as described above. sgRNA sequences used were *Fos* (UAGUGCCAAC-UUUAUCCCCA) and NTC (GCACUACCAGAGCUAACUCA).

Virus infection and viral titers

HSV-1 KOS was grown using Vero cells (CSL). Mice were epicutaneously infected with 10^6 plaque-forming units of HSV-1, as previously described[6].

Flow cytometry analysis of in vivo HSV-1 responses

Endogenous HSV-specific CD8$^+$ T cells were analyzed using H-2K^b-restricted gB$_{498–505}$-specific tetramers, as previously described[6]. In some experiments, *Ccl5*$^{-/-}$ and wild-type mice were transferred with 50,000 naive HSV-specific CD8$^+$ T cells (gBT-I cells) before infection, and their expansion was measured 10 days later in the spleen, as described previously[6]. IFNγ production in gB$_{498–505}$-specific CD8$^+$

T cells was measured after restimulation for 5 h ex vivo in the presence of brefeldin A. Single-cell suspensions were stained with antibodies to CD16/CD32 (2.4G2, Fc block), CD8 (53-6.7), CD44 (IM7), CD45.2 (104) and CD3 (145-2C11) and, when necessary, with either CD45.1 monoclonal antibody (A20) or tetramer staining. After fixation and permeabilization with BD Cytofix/Cytoperm (BD Biosciences), cells were stained for 20 min at room temperature with antibodies to IFNγ (XMG1.2) in BD Perm/Wash buffer (BD Biosciences) before analysis on a flow cytometer. Dead cells were excluded by using a LIVE/DEAD fixable dead cell stain kit (Thermo Fisher Scientific). A BD LSRFortessa and a FACS Diva or Biosciences Cytek Aurora and SpectroFlo were used for measurement of samples, and FlowJo software (TreeStar) was used for analysis. In some experiments, CD8$^+$ DCs from wild-type versus *Ifnar2*$^{-/-}$ mice were analyzed in the brachial lymph node 2 days after HSV-1 skin infection, as previously described[6]. Cells were stained with antibodies to CD11c (N418), CD8 (53-6.7), CD3 (145-2C11, BD Biosciences), CD19 (1D3), NK1.1 (PK136) and IA/E (2G9), and CD8$^+$ DCs were then processed on an analytic flow cytometer (LSRFortessa BD Biosciences).

BM chimeras

Mixed chimeras were generated as previously described[6]. C57BL/6 mice were lethally irradiated with 2×550 cGy and were reconstituted with a total of 5×10^6 bone marrow cells, previously depleted for T cells, from *Cxcr6*$^{-/-}$ and wild-type mice in a 1:1 ratio.

scRNA-seq data generation and analysis

scRNA-seq data of PBMCs from individuals with COVID-19 and healthy control individuals collected from April to July 2020 in Bonn, Germany, were used, as previously reported[26]. Samples were classified by disease severity according to the WHO ordinal scale (WHO score of 3, mild; WHO score of 4–5, moderate; WHO score of 7, severe) and by the time after onset of first symptoms (early: days 0–10, late: >day 11) at the date of sampling. Details about sample procurement and processing, sequencing and data analysis have been previously described[25], and an extensive description of the protocol has also been published[43]. Processed and annotated scRNA-seq data[25] were used as published previously and are available at https://beta.fastgenomics.org/p/schulte-schrepping_covid19. The data were imported into R version 4.0.3 and were mainly analyzed using Seurat v3.9.9.

Subset analysis of DCs and monocytes

PBMCs were subjected to Seurat v4 reference mapping following the developer vignette (satijalab.org/seurat/articles/multimodal_reference_mapping.html) using the multimodal PBMC reference data set[44]. Only those cells classified as DC or monocyte subsets were selected to remove any possible cellular contaminations in the data set. Subsequently, the remaining 37,100 cells were reclustered after scaling and regressing for unique molecular identifier (UMI) count per cell, identification of variable genes and PCA in this cellular subspace using the Louvain algorithm with a resolution of 0.2 based on the first 10 PCs. Clusters representing DCs or classical CD14$^+$ monocytes were then subsetted, respectively, and the resulting 31,736 monocytes and 722 DCs were analyzed in detail, including rescaling, identification of variable genes, PCA and subsequent UMAP based on the first 10 PCs. Disease severity-specific marker gene analysis was performed using the Wilcoxon rank-sum test with the following cutoffs: genes had to be expressed in more than 10% of the cells of the respective condition and exceed a logarithmic fold change cutoff of at least 0.2. Before dot plot visualization and functional enrichment analyses, sets of differentially expressed genes were filtered for ribosomal protein-coding genes (*RPL/RPS*), mitochondrial genes (MT-) and hemoglobin genes (*HBA1*, *HBA2* and *HBB*). Hallmark enrichment analysis of differentially expressed gene sets was performed using the Hallmark v7.3 database and the enricher function implemented in the R package clusterProfiler v3.18.0 (ref. 45). Gene set enrichment analyses of

'CD40-unresponsive', 'amplified' and 'combinatorial' gene signatures in the differentially expressed genes in monocytes from individuals with mild COVID-19 compared to those from individuals with severe disease were performed using the fgsea package v1.16.0. Single-sample GSVA using the 'CD40-unresponsive', 'amplified' and 'combinatorial' signatures derived from the mouse bulk RNA-seq analysis of this study was performed using GSVA v1.38.2 (ref. [46]). For this, aggregated expression values of all cells of each sample were calculated using the AggregateExpression function in Seurat and were used as input for the sample-specific analysis. Of note, the IFNαA response signature was intersected with the top 100 IFN-response genes derived from an integrated analysis of eight microarray data sets on IFN response of myeloid cells listed in the Interferome database (http://www.interferome.org/)[10] ranked by their combined $\log_2$(fold change) values to reduce the signature to a length comparable to the amplified and combinatorial signatures. Transcription factor binding motif enrichment analysis based on the significantly differentially expressed genes in monocytes derived from individuals with mild COVID-19 compared to cells from individuals with severe disease and those differentially expressed genes that intersected with the 'amplified' and 'combinatorial' gene signatures was performed using RcisTarget[32], the hg38__refseq-r80_10kb_up_and_down_tss.mc9nr.feather database and a normalized enrichment score threshold of 4. Enriched transcription factor binding motifs were filtered for the transfac_pro, cisbp and swissregulon databases and those motifs with high-confidence transcription factor annotation (TF_highConf). A network linking enriched target genes and predicted transcriptional regulators based on the Rcistarget transcription factor binding motif enrichment results was constructed and visualized in a circular layout using Cytoscape v3.7.1.

scRNA-seq analysis of CD14⁺ monocytes from individuals with IFN-AAB and corresponding healthy individuals

PBMC scRNA-seq data were produced from five control samples, five samples from individuals with moderate COVID-19, five samples from individuals with severe COVID-19 and seven samples from individuals with severe COVID-19 with IFN-AAB, which were tested for each individual in virus neutralization assays described in Akbil et al.[22]. On the day of the experiment, frozen live PBMCs were thawed in prewarmed medium (RPMI 1640 (Gibco), 2% fetal calf serum (Sigma) and 0.01% Pierce Universal Nuclease (Thermo Fisher)). The PBMCs were then labeled with 0.5 μg of TotalSeq-C hashtag antibodies (Biolegend) in DPBS supplemented with 0.5% BSA and 2 mM EDTA for 30 min at 4 °C and washed at least three times with DPBS + 1% BSA. Subsequently, the PBMCs were counted, and up to seven different samples were pooled in equal proportions. The resulting cell pool was filtered through a 40-μm mesh (Flowmi Cell Strainer, Merck) and super loaded with 50,000 cells per lane in the Chromium Controller for partitioning single cells into nanoliter-scale Gel Bead-In-Emulsions (GEMs). For reverse transcription, cDNA amplification and library construction of the gene expression libraries, the Chromium Next GEM Single Cell kit 5′ v2 (10x Genomics) was used. The Chromium Single Cell 5′ Feature Barcode Library kit (10x Genomics) was used for preparing additional hashtag libraries. All libraries were prepared according to the protocols provided by 10x Genomics, quantified by Qubit Flex fluorometer (Thermo Fisher) and quality checked using the 4150 TapeStation system. Sequencing was performed in paired-end mode (R1 26 cycles, R2 90 cycles) on a NovaSeq 6000 (Illumina) with a NovaSeq 6000 S2 reagent kit (100 cycles). After demultiplexing, raw sequencing data were processed with CellRanger v5 and aligned against the GRCh38 reference, including TotalSeq-C hashtag barcodes. scRNA-seq UMI count matrices were imported into R 4.0.3, and gene expression data analysis was performed using the R/Seurat package 3.9.9. Cells from pooled samples were demultiplexed using a combination of HTODemux implemented in Seurat and vireo (v0.5.6)[47] after scoring common variants from the 1000Genomes project with cellsnp-lite (v1.2.0)[48].

Events classified as 'negative' and 'doublet' by the HTODemux algorithm were assigned an ID via vireo classification. Subsequently, cells were filtered by number of features (over 200 and less than 5,000), percentage of mitochondrial genes (<10% mitochondrial UMIs) and number of counts per cell (<20,000) to exclude debris and doublets. Gene expression values were normalized by total UMI counts per cell, multiplied by 10,000 (TP10K) and log transformed by $\log_{10}$ (TP10k + 1). For cell-type annotation, cells were subjected to Seurat v4 reference mapping following the developer vignette using the multimodal PBMC reference data set[44]. Cells classified as CD14⁺ classical monocytes were selected and reclustered after scaling and identification of variable genes using vst and PCA using the Louvain algorithm with a resolution of 0.2 based on the first 10 PCs. A cluster characterized by the expression of T cell marker genes was removed to exclude potential T cell contamination in the CD14⁺ monocyte subset. Averaged gene expression values per sample of selected key genes were visualized as box plots across disease severity groups.

To increase the number of samples per severity group, scRNA-seq data of PBMCs from other COVID-19 cohorts produced using the same scRNA-seq protocol (10x Genomics, 5′) by us[21] and others[27,28] were included in the analysis and processed as described above. The total number of samples combined in this analysis was 263. All samples were grouped according to their WHO ordinal scale classification into mild (WHO score of 1–3), moderate (WHO score of 4–5) and severe (WHO score of 6–8) COVID-19 disease. In addition, samples known to be derived from individuals with IFN-AAB were subgrouped accordingly. PBMC scRNA-seq data from Van der Wijst et al.[28] were downloaded and filtered for the earliest sample available per donor, resulting in 11 control samples and 35 samples from individuals with moderate COVID-19, 26 samples from individuals with severe COVID-19 and 4 samples from individuals with severe COVID-19 with IFN-AAB. PBMC scRNA-seq data from Su et al.[27] were downloaded and filtered for the earliest sample available per donor, resulting in 17 control samples and 69 samples from individuals with mild COVID-19, 45 samples from individuals with moderate COVID-19 and 15 samples from individuals with severe COVID-19. PBMC scRNA-seq data from Georg et al.[21] included six control samples, five samples from individuals with mild COVID-19, two samples from individuals with moderate COVID-19 and six samples from individuals with severe COVID-19. Single-sample GSVA using the 'CD40-unresponsive', 'amplified' and 'combinatorial' signatures derived from the mouse bulk RNA-seq analysis of this study was performed using GSVA v1.38.2.

For validation, we additionally analyzed scRNA-seq data from DCs from PBMC data enriched for DCs as previously published[26]. After downloading the respective data from the public domain, we selected those cells originally classified as monocytes and DCs and followed the same procedure of filtering the cells using the Seurat v4 reference mapping approach, as outlined above. Differential gene expression analyses and signature enrichment analyses of the 'CD40-unresponsive', 'amplified' and 'combinatorial' signatures were performed as described above.

Subset analysis of CD8⁺ T cells

For detailed analysis of the CD8⁺ T cell compartment, cells classified as T cells according to the original annotation provided were selected from the PBMC data set. These cells were subjected to Seurat v4 reference mapping following the developer vignette (satijalab.org/seurat/articles/multimodal_reference_mapping.html) using the multimodal PBMC reference data set[44]. Only those cells classified as T cells were selected to remove any possible cellular contaminations in the T cell data set. Subsequently, the remaining 45,516 cells were reclustered after scaling, regressing for UMI count per cell, identification of variable genes and PCA in this cellular subspace using the Louvain algorithm with a resolution of 0.2 based on the first 10 PCs. Cluster 1, representing CD8⁺ T cells, was then subsetted, and the resulting 12,386 cells were analyzed in detail, including rescaling, identification of variable

genes, PCA and subsequent UMAP[49] based on the first 10 PCs. Ribosomal protein-coding genes (*RPL/RPS*), mitochondrial genes (MT-) and hemoglobin genes (*HBA1*, *HBA2* and *HBB*) were excluded from the set of variable features to remove potential sources of technical differences. Single-sample GSVA using the 'helped' and 'unhelped' T cell signatures derived from RNA-seq analysis of CD8^{+} T cells primed in the presence or absence of CD4^{+} T cell responses was performed using GSVA v1.38.2. For this, aggregated expression values of all CD8^{+} T cells of each sample were calculated using the AggregateExpression function in Seurat and were used as input for the sample-specific analysis. Clustering of the CD8^{+} T cells was performed using the Louvain algorithm with a resolution of 0.4 based on the first 10 PCs, and cells identified as γδT cells were removed. To investigate proportional cluster occupancy per disease severity, cell counts per condition were normalized before calculation of per-cluster percentages. Single-cell gene set enrichment analysis across cells of each CD8^{+} T cell subcluster using the 'helped' and 'unhelped' T cell signatures derived from RNA-seq analysis of CD8^{+} T cells primed in the presence or absence of CD4^{+} T cell responses was performed using AUCell v1.12.0 (ref. [32]). For validation, we analyzed CD8^{+} T cells from two other data sets[36,37]. After downloading the respective data from the public domain, we followed the same procedure of filtering the cells using the Seurat v4 reference mapping approach and performed signature enrichment analysis using the above-mentioned T cell signatures.

Analysis of scATAC-seq data
scATAC-seq data of PBMCs from individuals with COVID-19 and healthy individuals produced using a Chromium Next GEM Single Cell ATAC reagent kit version 1.1 (10x Genomics, PN-1000175) was used, as previously published[29]. Processed and annotated scATAC-seq data from Wilk et al.[29] were downloaded from Gene Expression Omnibus (GEO) under accession number GSE174072 and https://github.com/ajwilk/COVID_scMultiome and were imported to R version 4.1.0. After creation of Arrow files and a respective ArchRproject using the R package ArchR version 1.0.1 (ref. [50]), the resulting single-cell data were filtered based on the published cell annotation and subsetted to CD14^{+} monocytes. Imputation weights on GeneScores were calculated using MAGIC[51] implemented in ArchR's addImputeWeights function. Severity-specific accessible genes were identified using the Wilcoxon rank-sum test comparing gene scores of monocytes from individuals with mild COVID-19 to cells from control donors with the following cutoffs: FDR ≤ 0.05 and $\log_2$(fold change) ≥ 0.58. Hallmark enrichment analyses were performed using clusterProfiler version 4.0.5 and the Hallmark gene set v6.2. After generation of pseudo-bulk replicates across cells of each COVID-19 severity group, peaks were called using MACS3 (ref. [52]) and annotated using ChIPseeker version 1.28.3 (ref. [53]). Subsequently, transcription factor binding motifs were identified in the peak regions using the homer motif set. After calculation of severity-specific differentially accessible peak regions (FDR ≤ 0.01 and $\log_2$(fold change) ≥ 2) comparing chromatin profiles of monocytes from individuals with mild and severe COVID-19 to cells from control donors, motif enrichment analysis was performed using ArchR's peakAnnoEnrichment function.

CyTOF data and analysis
For mass cytometry data from a publicly available publication[21], please refer to the Methods part of the work for detailed descriptions of the cohort, data collection and analysis workflows. Here, CD8^{+} T cells were separately reanalyzed and pregated using OMIQ cloud-based cytometry analysis software, also in relation to the presence of IFN-AAB[22]. In addition to the steps described[21], we performed a PCA using R (4.0.2), where principal components were first calculated for all the events, and averages of principal component values per individual were used in plotting. Figures were rendered with the help of the R package ggfortify and function autoplot, which allows plotting of eigenvectors of input variables when used on precalculated principal components.

An ellipse was calculated with ggplot2 to visually estimate the localization of different groups. Marker intensity box plots show average z-score-normalized intensity signals for all the CD8^{+} T cells per individual. Z-score normalization was performed beforehand over all the immune cells acquired in CyTOF.

Flow cytometry analysis of monocytes and DCs in individuals with COVID-19
Fixed whole-blood samples from individuals with COVID-19 were collected, processed and stored, as previously described[25]. The samples were subsequently thawed to room temperature, and erythrocytes were lysed with Thaw-Lysis buffer (Smart Buffer). After 5 min of treatment with 50 U ml^{-1} Pierce Universal Nuclease for Cell Lysis (Thermo Scientific) and 20 min of blocking with 1 mg ml^{-1} beriglobin (CSL Behring), the samples were stained for 30 min at 4 °C with antibodies to CD45 (HI30), CD11c (Bu15), CD14 (MφP9), CD3 (UCHT1), CD19 (SJ25C1), CD40 (5C3), CD83 (HB15e), CD86 (IT2.2), HLA-DR (G46-6), CD16 (3G8), CD141 (1A4) and CD163 (GHI/61). A BD LSRFortessa was used for the measurement of samples, and FlowJo software (TreeStar) was used for analysis. Expression of CD45, CD3, CD19 and HLA-DR was used for granulocyte, T cell, B cell and natural killer cell exclusion, respectively. Monocytes were gated as CD14^{+}CD11c^{+} and DCs as CD14^{−}HLA-DR^{+} events.

In vitro generation of human CD34^{+} stem cell-derived cDC1s
Human umbilical cord blood was obtained with written informed consent from the Queensland Cord Blood Bank and approval from the Mater Human Research Ethics Committee (HREC13/MHS/86). cDC1s were differentiated in a 9- to 10-d culture of in vitro expanded cord blood CD34^{+} progenitors in 100 ng ml^{-1} FLT3L (Peprotech), 100 ng ml^{-1} stem cell factor (Peprotech), 2.5 ng ml^{-1} IL-4 (Invitrogen) and 2.5 ng ml^{-1} granulocyte–macrophage colony-stimulating factor (Invitrogen), as previously described[30], but with the addition of an irradiated OP9-DL1 stromal cell feeder layer to maximize cDC1 yields[54]. CD141^{+}CADM1^{+}CLEC9A^{+} cDC1s were enriched to >80% purity by labeling with biotinylated antibodies to human CADM1 (CM004-6) or CD141 (M80) and anti-biotin microbeads, followed by positive selection on an LS column according to manufacturer's instructions (Miltenyi). Purified cDC1s were cultured at a density of 1×10^6 per ml in the presence of 1,000 U ml^{-1} human IFNα2a (PBL), 5 μg ml^{-1} CD40 agonistic antibody[11] (34G12-h2, a gift from M. Cragg at University of Southhampton) or a combination. TNF-α was detected in the supernatant after 18 h using a LegendPlex kit (Biolegend) on a CytoFLEX-S (Beckman Coulter) flow cytometer.

Quantification and statistical analysis
Prism v8.4.3 (GraphPad Software) was used to assess statistical significance of non-RNA-seq data; z score = $(x − \text{mean})/\text{s.d.}$ The sample size (*n*), statistical significance and statistical tests are indicated in the legends. Data distribution was assumed to be normal, but this was not formally tested. Data collection and analysis were not performed blind to the conditions of the experiments and no formal randomization was used. No data points were excluded.

Reporting summary
Further information on research design is available in the Nature Portfolio Reporting Summary linked to this article.

Data availability
The RNA-seq data set generated in this study can be accessed via the GEO accession number GSE171690.

Code availability
Code used for the analysis of scRNA-seq and scATAC-seq data is available at https://github.com/schultzelab/Gressier_2022. We also provide

the scRNA-seq data sets used in this study and the code to analyze the respective data sets via FASTGenomics (https://beta.fastgenomics.org/p/gressier_2022).

References

38. Kurth, F. et al. Studying the pathophysiology of coronavirus disease 2019: a protocol for the Berlin prospective COVID-19 patient cohort (Pa-COVID-19). *Infection* **48**, 619–626 (2020).
39. Huang da, W., Sherman, B. T. & Lempicki, R. A. Systematic and integrative analysis of large gene lists using DAVID bioinformatics resources. *Nat. Protoc.* **4**, 44–57 (2009).
40. Subramanian, A. et al. Gene set enrichment analysis: a knowledge-based approach for interpreting genome-wide expression profiles. *Proc. Natl Acad. Sci. USA* **102**, 15545–15550 (2005).
41. Kaya-Okur, H. S. et al. CUT&Tag for efficient epigenomic profiling of small samples and single cells. *Nat. Commun.* **10**, 1930 (2019).
42. Freund, E. C. et al. Efficient gene knockout in primary human and murine myeloid cells by non-viral delivery of CRISPR–Cas9. *J. Exp. Med.* **217**, e20191692 (2020).
43. De Domenico, E. et al. Optimized workflow for single-cell transcriptomics on infectious diseases including COVID-19. *STAR Protoc.* **1**, 100233 (2020).
44. Hao, Y. et al. Integrated analysis of multimodal single-cell data. *Cell* https://doi.org/10.1016/j.cell.2021.04.048 (2021).
45. Wu, T. et al. clusterProfiler 4.0: a universal enrichment tool for interpreting omics data. *Innovation* **2**, 100141 (2021).
46. Hanzelmann, S., Castelo, R. & Guinney, J. GSVA: gene set variation analysis for microarray and RNA-seq data. *BMC Bioinformatics* **14**, 7 (2013).
47. Huang, Y., McCarthy, D. J. & Stegle, O. Vireo: Bayesian demultiplexing of pooled single-cell RNA-seq data without genotype reference. *Genome Biol.* **20**, 273 (2019).
48. Huang, X. & Huang, Y. Cellsnp-lite: an efficient tool for genotyping single cells. *Bioinformatics* **37**, 4569–4571 (2021).
49. McInnes, L., Healy, J. & Melville, J. UMAP: Uniform Manifold Approximation and Projection for dimension reduction. Preprint at https://doi.org/10.48550/arXiv.1802.03426 (2018).
50. Granja, J. M. et al. ArchR is a scalable software package for integrative single-cell chromatin accessibility analysis. *Nat. Genet.* **53**, 403–411 (2021).
51. van Dijk, D. et al. Recovering gene interactions from single-cell data using data diffusion. *Cell* **174**, 716–729 (2018).
52. Zhang, Y. et al. Model-based analysis of ChIP–seq (MACS). *Genome Biol.* **9**, R137 (2008).
53. Yu, G., Wang, L. G. & He, Q. Y. ChIPseeker: an R/Bioconductor package for ChIP peak annotation, comparison and visualization. *Bioinformatics* **31**, 2382–2383 (2015).
54. Balan, S. et al. Large-scale human dendritic cell differentiation revealing notch-dependent lineage bifurcation and heterogeneity. *Cell Rep.* **24**, 1902–1915 (2018).

Author contributions

Conceptualization: S. Bedoui, E.G., J.S.-S. and S.V.S. Methodology: P.G.W., A.B., K.H., M.K., M. Clarke, T.H.O.N., P.S., K.W., C.V.L.O., B.O., C.v.d.S., Y.-C.E.C., K.J.R., T.M., M. Chopin, S. Brumhard, S.S.G., K.K. and S.L.L. Formal analysis: E.G., J.S.-S., A.O., J. Spitzer, L.J.G., P.J.H., L.P., T.K., T.A., F.K., J. Schroeder and B.S. Investigation: E.G., J.S.-S., P.G.W., A.B., M.G. and F.K. Writing, original draft: S. Bedoui and E.G. Writing, review and editing: S. Bedoui, E.G., J.S.-S., S.V.S., J.L.S., W.K., A.K., T.G., E.L., C.K. and L.E.S. Funding acquisition: S. Bedoui, T.G., E.L., J.L.S. and S.V.S.

Competing interests

The authors declare no competing interests.

Additional information

Extended data is available for this paper at https://doi.org/10.1038/s41590-023-01517-x.

Supplementary information The online version contains supplementary material available at https://doi.org/10.1038/s41590-023-01517-x.

Correspondence and requests for materials should be addressed to Elise Gressier or Sammy Bedoui.

Peer review information *Nature Immunology* thanks Teunis Geijtenbeek, and the other, anonymous, reviewer(s) for their contribution to the peer review of this work. Primary Handling Editor: Ioana Visan, in collaboration with the *Nature Immunology* team. Peer reviewer reports are available.

Reprints and permissions information is available at www.nature.com/reprints.
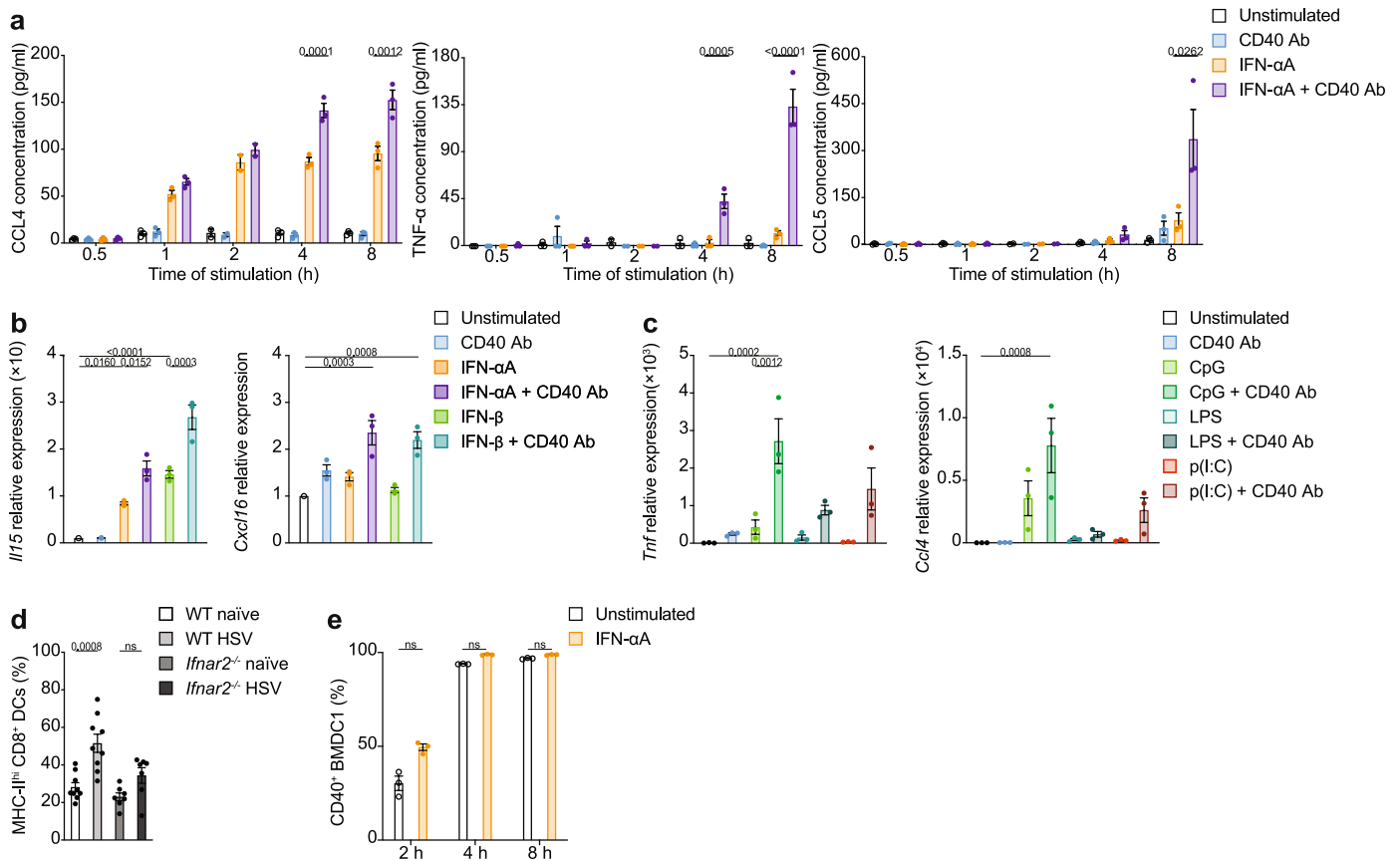
Extended Data Fig. 1 | CD40 synergizes with varying inflammatory stimuli BMDC1. a, 'BMDC1-IFN-αA+CD40' increase secretion of CCL4, TNF-α and CCL5 (from left to right) over time compared to 'BMDC1-IFN-αA', 'BMDC1-CD40' and 'BMDC1-unstimulated'. Data are presented as mean ± s.e.m pooled from 3 independent experiments. Adjusted p-value of statistically significant differences between conditions as assessed by one-way ANOVA indicated. **b**, Changes in *Il15* and *Cxcl16* expression in 'BMDC1-IFN-αA+CD40' and 'BMDC1-IFN-β+CD40' compared to 'BMDC1-IFN-αA' or 'BMDC1-IFN-β' respectively and to 'BMDC1-CD40' and 'BMDC1-unstimulated'. **c**, *Tnf* and *Ccl4* in expression in BMDC1s stimulated with LPS, CpG or poly(I:C) for 6 h with or without CD40 Ab for the last 30 min. **b-c**, Data are presented as mean ± s.e.m pooled from

3 independent experiments. Adjusted p-value of statistically significant differences between conditions as assessed by one-way ANOVA indicated; ns = non-significant. **d**, Percent of MHC-II^hi CD8^+ DCs from IFNαR-deficient (*Ifnar2^−/−*) and WT mice naïve or 2 days after epicutaneous HSV-1 infection. Data are presented as mean ± s.e.m pooled from 7 independent experiments (n≥5 per experiment). Statistically significant differences between conditions as assessed by Mann-Whitney test; two-tailed p-value indicated; ns = non-significant. **e**. 'BMDC1-IFN-αA' and 'BMDC1-unstimulated' increase CD40 expression to comparable levels over time. Data are presented as mean ± s.e.m pooled from 3 independent experiments. Two-way ANOVA performed between the corresponding conditions ns = non-significant.
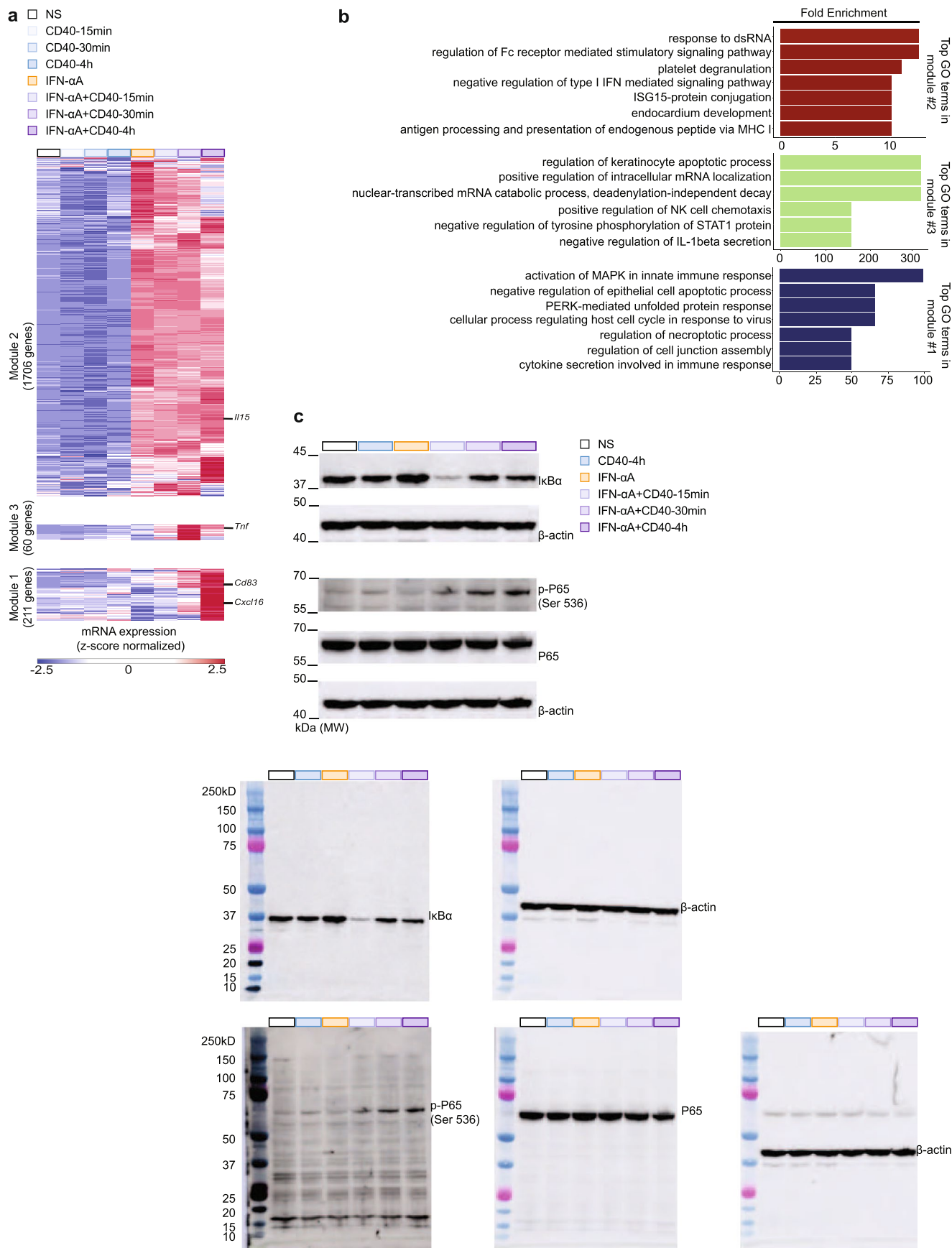
**Extended Data Fig. 2 | See next page for caption.**

Extended Data Fig. 2 | CD40 stimulation induces successive waves of transcriptional regulation in IFN-αA-conditioned BMDC1. a, Genes included in modules 1, 2 and 3 from the co-expression analysis (Fig. 2e) displayed as heatmap. **b**, Top GO-terms associated with the genes included in modules 1, 2 and 3 (Fig. 2e). **c**, Representative immunoblotting of IκBα degradation and P65 phosphorylation in 'BMDC1-IFNαA+CD40-15min', 'BMDC1-IFNαA-30min' and 'BMDC1-IFN-αA+CD40-4h' compared to 'BMDC1-IFN-αA', 'BMDC1-CD40' and 'BMDC1-unstimulated'. Full gels of the two independent experiments are displayed below. Probing of β-actin and/or total P65 served as loading control.
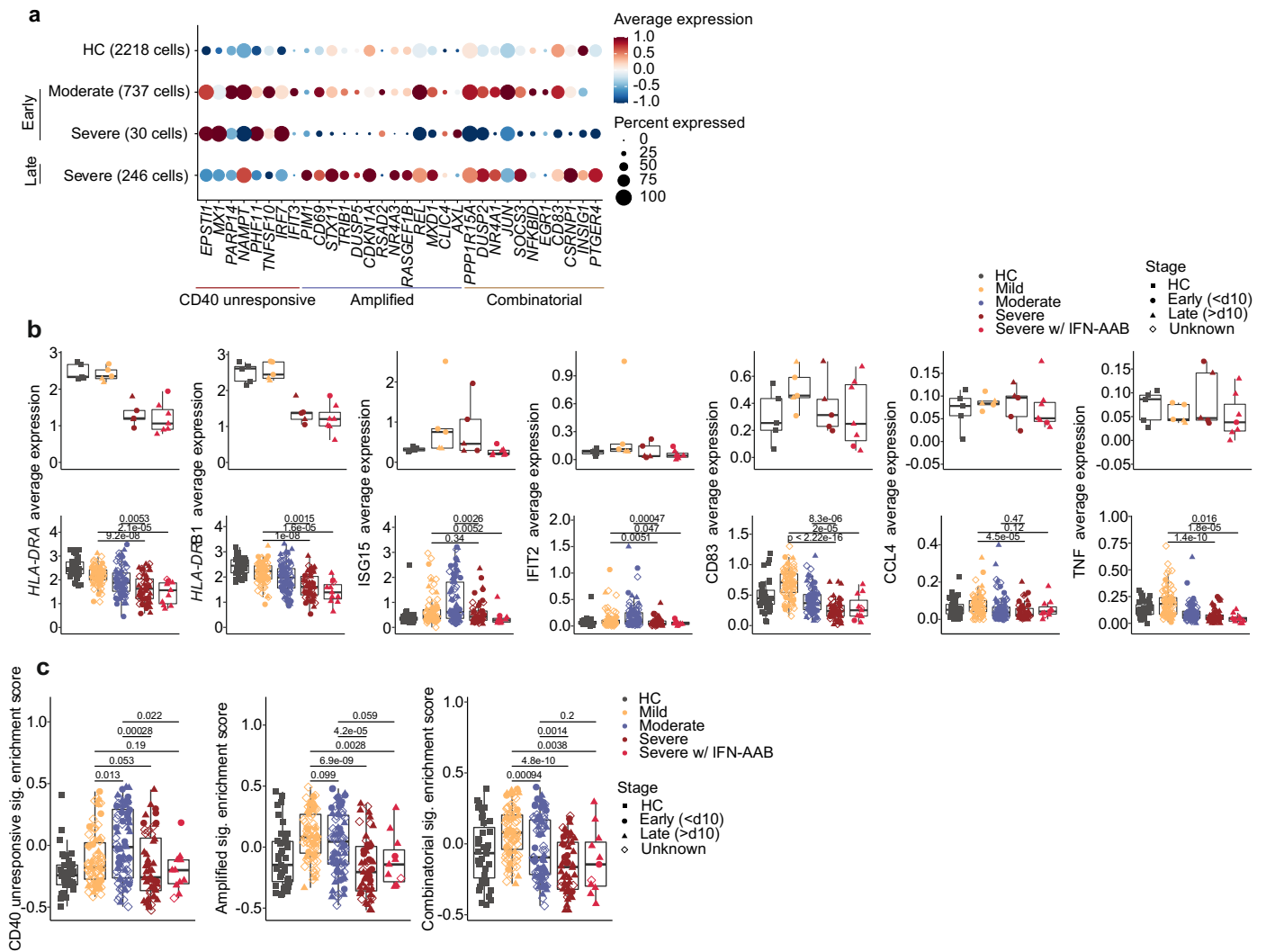
Extended Data Fig. 3 | Enrichment of APC with 'help'-dependent transcriptional profiles in patients with moderate COVID-19. a, Differentially expressed genes in DCs comparing disease severity and disease stage that correspond to the 'CD40 unresponsive', 'amplified' and 'combinatorial'. Data from published DC-enriched scRNAseq data[26]. **b**, Average gene expression in CD14^{+} monocytes per sample across selected key genes in a cohort of control (n=5), mild (n=5) and severe (n=5) COVID-19 patients and 7 samples derived from patients with IFN-AAB. **c**. Combined data set across 263 samples including controls (n=39), mild COVID-19 (WHO 1-3, n=79), moderate COVID-19 (WHO

4-5, n=82), severe COVID-19 (WHO 6-8, n=52), severe COVID-19 with IFN-AAB (WHO 7-8, n=11). Samples are stratified by disease severity according to the WHO ordinal scale as indicated and segregated by time point of sample collection relative to the onset of symptoms where available. **c**, Single-sample GSVA of the 'CD40 unresponsive', 'amplified' and 'combinatorial' gene signatures in monocytes from COVID-19 and control samples of the combined data set in b. stratified by disease severity and plotted as box plots of the enrichment scores. Wilcoxon rank-sum test p-value is shown.
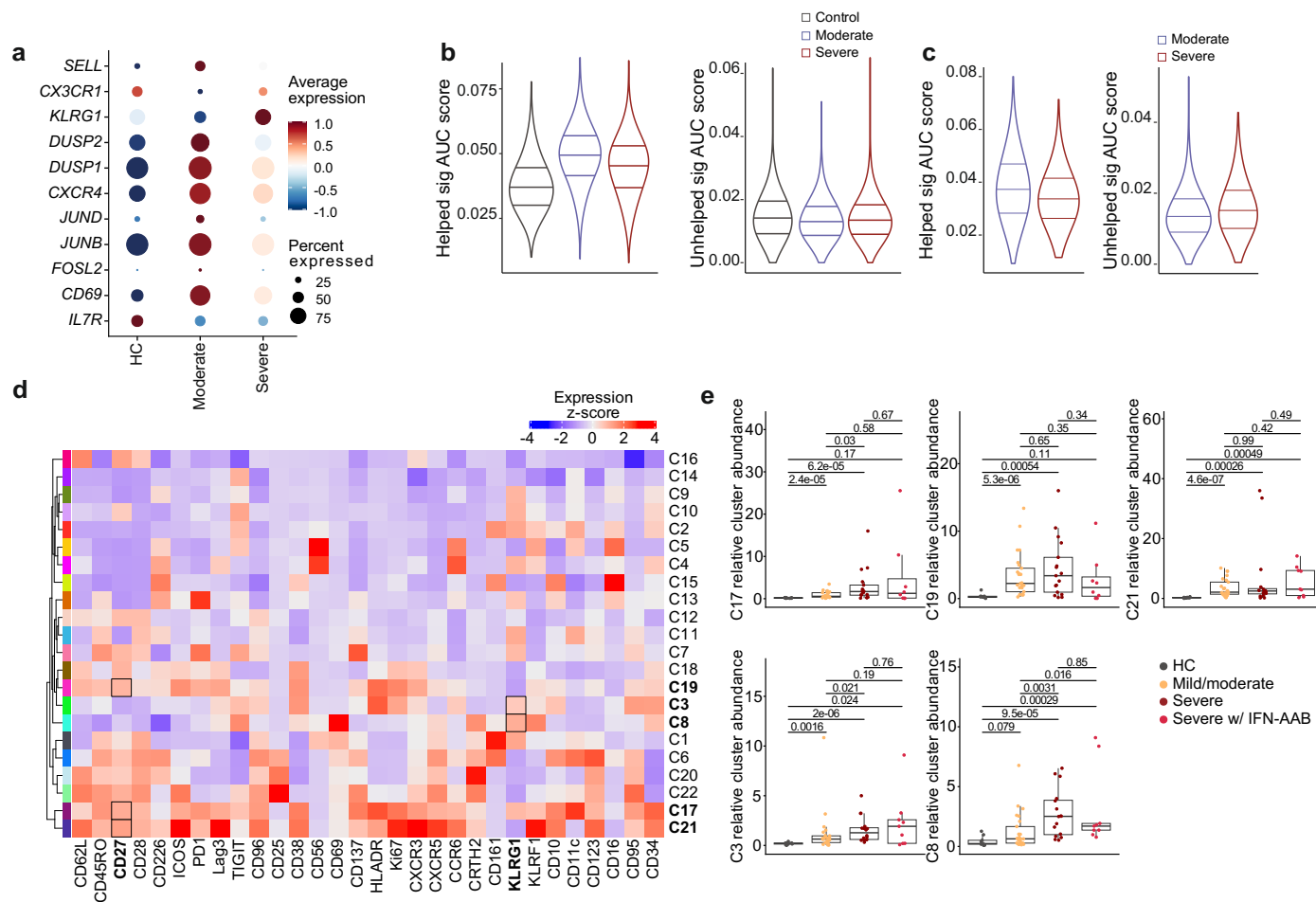
Extended Data Fig. 4 | Enrichment of CD8⁺ T cells with 'help'-dependent transcriptional profiles in patients with moderate COVID-19. a, Differential expression of selected key genes in CD8⁺ T cells derived from PBMCs scRNA-seq data of moderate and severe cases of COVID-19 and healthy HC originally as published[36]. **b**, AUCell enrichment of CD8⁺ T cells for 'helped' and 'unhelped' T cell gene signatures derived from RNA-seq analysis of CD8⁺ T cells primed in the presence or absence of CD4⁺ T cell help. Data are stratified by disease severity and plotted as violin plots of the 'Area Under the Curve' (AUC) scores. **c**. AUCell enrichment of CD8⁺ T cells for 'helped' and 'unhelped' T cell gene signatures

derived from RNA-seq analysis of CD8⁺ T cells primed in the presence or absence of CD4⁺ T cell help. Data are derived from scRNA-seq of nasopharyngeal and bronchial samples stratified by disease severity and plotted as violin plots of the 'Area Under the Curve' (AUC) scores[37]. **d**, Heatmap showing z-scaled expression values of indicated proteins across the clusters identified in the CyTOF data of individuals with COVID-19 and HCs. **e**, Box plots showing relative cluster abundances of selected clusters across COVID-19 and control samples stratified according to disease severity and presence of IFN-AAB. Benjamini-Hochberg corrected pairwise Wilcoxon p-values are shown.

nature portfolio

Corresponding author(s):	Sammy Bedoui
Last updated by author(s):	13/04/2023

Reporting Summary

Nature Portfolio wishes to improve the reproducibility of the work that we publish. This form provides structure for consistency and transparency in reporting. For further information on Nature Portfolio policies, see our Editorial Policies and the Editorial Policy Checklist.

Statistics

For all statistical analyses, confirm that the following items are present in the figure legend, table legend, main text, or Methods section.

n/a	Confirmed	
☐	☒	The exact sample size (n) for each experimental group/condition, given as a discrete number and unit of measurement
☐	☒	A statement on whether measurements were taken from distinct samples or whether the same sample was measured repeatedly
☐	☒	The statistical test(s) used AND whether they are one- or two-sided *Only common tests should be described solely by name; describe more complex techniques in the Methods section.*
☒	☐	A description of all covariates tested
☐	☒	A description of any assumptions or corrections, such as tests of normality and adjustment for multiple comparisons
☐	☒	A full description of the statistical parameters including central tendency (e.g. means) or other basic estimates (e.g. regression coefficient) AND variation (e.g. standard deviation) or associated estimates of uncertainty (e.g. confidence intervals)
☐	☒	For null hypothesis testing, the test statistic (e.g. F, t, r) with confidence intervals, effect sizes, degrees of freedom and P value noted *Give P values as exact values whenever suitable.*
☒	☐	For Bayesian analysis, information on the choice of priors and Markov chain Monte Carlo settings
☒	☐	For hierarchical and complex designs, identification of the appropriate level for tests and full reporting of outcomes
☐	☒	Estimates of effect sizes (e.g. Cohen's d, Pearson's r), indicating how they were calculated

Our web collection on statistics for biologists contains articles on many of the points above.

Software and code

Policy information about availability of computer code

Data collection	Murine experiments: FACS Diva software (LSR Fortessa) and SpectroFlo (Cytek Aurora); HiSeq (Illumina), NovaSeq 6000 (Illumina), BD Rhapsody Single-Cell Analysis System (BD Biosciences). Single-cell RNA sequencing count data of PBMC from COVID-19 patients and controls collected from April to July 2020 in Bonn, Germany, was used as previously published in Schulte-Schrepping et al., 2020 Cell (doi: 10.1016/j.cell.2020.08.001). Furthermore, we used publically available scRNA-seq count data from Arunachalam et al., 2020 Science (doi:10.1126/science.abc6261), Bernardes et al., 2020 Immunity (doi:10.1016/j.immuni.2020.11.017) and Chua et al., 2020 Nat Biotechnol (doi:10.1038/s41587-020-0602-4). All count data was downloaded as published in the respective original publication. Details on data production and processing, incl. alignment and quantification, can be found in the respective paper.
Data analysis	FlowJo v.10.7.1, GraphPad Prism v.8, ImageJ v1.53a, STAR v2.5.3a, PartekFlow v8.0.19.0707, Partek Genomics Suite v7.18.0402, GSEA application v4.0.3, ggplot2 v3.3.3, BioLayout Express3D v3.3, BiNGO v3.0.3, EnrichmentMap v3.2.1, WordCloud plugin v3.1.3, WGCNA R package v1.70-3, Cytoscape v3.7.1, plugin iRegulon v1.3; Seurat v3.9.9 & v4, R v4.0.3, HALLMARK v7.3, Clusterprofiler v3.18.0, v4.05 & v3.18.0, AUCell v1.12.0 and RcisTarget in R version 4.0.3, 4.1.0 & 4.0.2. The respective code used for the analysis of scRNA-seq data will be made available at https://github.com/schultzelab/Gressier_2021. Furthermore, public scRNA-seq datasets utilized in this study as well as the code to analyze the respective data sets will be provided via the interactive online plattform for single-cell genomics FASTGenomics.

For manuscripts utilizing custom algorithms or software that are central to the research but not yet described in published literature, software must be made available to editors and reviewers. We strongly encourage code deposition in a community repository (e.g. GitHub). See the Nature Portfolio guidelines for submitting code & software for further information.

Data

Policy information about availability of data

All manuscripts must include a data availability statement. This statement should provide the following information, where applicable:

- Accession codes, unique identifiers, or web links for publicly available datasets
- A description of any restrictions on data availability
- For clinical datasets or third party data, please ensure that the statement adheres to our policy

Murine experiments: The RNA-seq dataset generated within this study concerning Figures 1 to 3 can be accessed via the GEO accession number: GSE171690 (https://www.ncbi.nlm.nih.gov/geo/query/acc.cgi?acc=GSE171690, Token: odqlweqyzlsnhix).

Human scRNA sequencing: Publically available scRNA-seq count data analyzed in this manuscript has been downloaded for Schulte-Schrepping et al., 2020 Cell (doi: 10.1016/j.cell.2020.08.001, data: https://beta.fastgenomics.org/p/schulte-schrepping_covid19), Arunachalam et al., 2020 Science (doi:10.1126/science.abc6261, data: GSE155673), Bernardes et al., 2020 Immunity (doi:10.1016/j.immuni.2020.11.017, data: shared upon request, https://beta.fastgenomics.org/p/565003) and Chua et al., 2020 Nat Biotechnol (doi:10.1038/s41587-020-0602-4, data: https://doi.org/10.6084/m9.figshare.12436517).

Field-specific reporting

Please select the one below that is the best fit for your research. If you are not sure, read the appropriate sections before making your selection.

☒ Life sciences ☐ Behavioural & social sciences ☐ Ecological, evolutionary & environmental sciences

For a reference copy of the document with all sections, see nature.com/documents/nr-reporting-summary-flat.pdf

Life sciences study design

All studies must disclose on these points even when the disclosure is negative.

Sample size	Murine experiments: in vitro experiments: the sample size of each sample/condition was robust; in vivo experiments sample size included a minimum of 3-5 mice for each experiment. In both cases, data were routinely collected across at least 2 independent replicates for each assay.
Data exclusions	Murine experiments: No data were excluded.
Replication	Murine experiments: 2-4 independent repeats were performed for each experiment with independent in vitro cultures or independent sets of mice for in vivo experiments. All replication attempts were successful.
Randomization	Murine experiments: No formal randomization was performed, specific in vitro conditions were applied to cell samples originating from the same source and in vivo comparisons were done across mice of different genotypes, not across mice of the same genotypes receiving different treatments.
Blinding	Murine experiments: N/A, investigators were not blinded to experimental conditions (in vitro experiments required prior knowledge for experimental set up).

Reporting for specific materials, systems and methods

We require information from authors about some types of materials, experimental systems and methods used in many studies. Here, indicate whether each material, system or method listed is relevant to your study. If you are not sure if a list item applies to your research, read the appropriate section before selecting a response.

Materials & experimental systems

n/a	Involved in the study
☐	☒ Antibodies
☒	☐ Eukaryotic cell lines
☒	☐ Palaeontology and archaeology
☐	☒ Animals and other organisms
☐	☒ Human research participants
☒	☐ Clinical data
☒	☐ Dual use research of concern

Methods

n/a	Involved in the study
☐	☒ ChIP-seq
☐	☒ Flow cytometry
☒	☐ MRI-based neuroimaging

Antibodies

Antibodies used	Murine cells sort: CD45R/B220 (RA3-6B2 - BD Pharmigen #558108), SIRPa (P84 - eBioscience #17-1721-82 or BD OptiBuild #740159),

Antibodies used	CD11c (N418 - eBioscience #25-0114-82), CD11b (M1/70 - BioLegend #101242), I-A/E (M5114 - eBioscience #56-5321-82), CD24 (M1/69 - BioLegend #101806) antibodies.
	Murine cells stimulation: anti-CD40 monoclonal antibody (FGK45.5 - Miltenyi Biotec #130-093-023).
	BD Cytometric Bead Array measurement: antibodies from the respective flex sets for the measurement of mouse CCL4 (MIP-1b - #558343), mouse CCL5 (RANTES - #558345), mouse IL-6 (#558301) and mouse TNF-a (#558299), all purchased from BD Biosciences.
	Western Blot: rabbit anti-NF-kB p65 (D14E12, #8242), mouse anti-phospho S536 NF-kB p65 (7F1, #3036), rabbit anti-IkBa (44D4, #4812) and rabbit anti-b-actin (13E5, #4970); anti-rabbit IgG, HRP-linked antibody (#7074) and anti-mouse IgG, HRP-linked antibody (#7076), all purchased from Cell Signaling Technology.
	PhosFlow cytometry: Phospho-p44/42 MAPK (Erk1/2) (Thr202/Tyr204) antibody (197G2 - Cell Signaling Technology #13148) and Phospho-p38 MAPK (Thr180/Tyr182) antibody (4NIT4KK - ThermoFisher Scientific #46-9078-42).
	Flow Cytometry following HSV infection and restimulation: CD16/CD32 (2.4G2, Fc block - BD Pharmigen #553142), CD8 (53-6.7 - eBioscience #17-0081-82), CD44 (IM7 - eBioscience #45-0441-82), CD45.2 (104- eBioscience #47-0454-82), CD3 (145-2C11 - BD Horizon #563565), IFN-g (XMG1.2 - BD Biosciences #557649) antibodies.
Validation	The antibodies are all in common use and have been validated by the manufacturer and by citations. Validation materials are available on respective manufacturer home pages for each antibody.
	Isotype controls (for anti-CD40 monoclonal antibody, FGK45.5 from Miltenyi Biotec) and Fluorescence Minus One (FMO) for Phospho-p44/42 MAPK (Erk1/2) (Thr202/Tyr204) and Phospho-p38 MAPK (Thr180/Tyr182) were used to perform validation in these specific circumstances.

Animals and other organisms

Policy information about studies involving animals; ARRIVE guidelines recommended for reporting animal research

Laboratory animals	C57BL/6, Cd40-/-, Irf1-/- and Cxcr6-/- mice used in this study were all female between 6 and 12 weeks of age.
Wild animals	This study did not involve wild animals.
Field-collected samples	This study did not involve samples collected in the field.
Ethics oversight	All animal experiments were approved by The University of Melbourne Animal Ethics Committee

Note that full information on the approval of the study protocol must also be provided in the manuscript.

Human research participants

Policy information about studies involving human research participants

Population characteristics	Population characteristics on the human research participants included in the respective cohorts of the PBMC single-cell RNA sequencing data sets included in this manuscript can be found in the original publications: Schulte-Schrepping et al., 2020 Cell (doi: 10.1016/j.cell.2020.08.001), Arunachalam et al., 2020 Science (doi:10.1126/science.abc6261), Bernardes et al., 2020 Immunity (doi:10.1016/j.immuni.2020.11.017) and Chua et al., 2020 Nat Biotechnol (doi:10.1038/s41587-020-0602-4).
Recruitment	Details on the recruitment of the human research participants included in the respective cohorts of the PBMC single-cell RNA sequencing data sets included in this manuscript can be found in the original publications: Schulte-Schrepping et al., 2020 Cell (doi: 10.1016/j.cell.2020.08.001), Arunachalam et al., 2020 Science (doi:10.1126/science.abc6261), Bernardes et al., 2020 Immunity (doi:10.1016/j.immuni.2020.11.017) and Chua et al., 2020 Nat Biotechnol (doi:10.1038/s41587-020-0602-4).
Ethics oversight	Details on the ethical oversight of the respective cohorts of the PBMC single-cell RNA sequencing data sets included in this manuscript can be found in the original publications: Schulte-Schrepping et al., 2020 Cell (doi: 10.1016/j.cell.2020.08.001), Arunachalam et al., 2020 Science (doi:10.1126/science.abc6261), Bernardes et al., 2020 Immunity (doi:10.1016/j.immuni.2020.11.017) and Chua et al., 2020 Nat Biotechnol (doi:10.1038/s41587-020-0602-4).

Note that full information on the approval of the study protocol must also be provided in the manuscript.

ChIP-seq

Data deposition

☒ Confirm that both raw and final processed data have been deposited in a public database such as GEO.

☐ Confirm that you have deposited or provided access to graph files (e.g. BED files) for the called peaks.

Data access links	*For "Initial submission" or "Revised version" documents, provide reviewer access links. For your "Final submission" document,*
May remain private before publication.	*provide a link to the deposited data.*
Files in database submission	*Provide a list of all files available in the database submission.*
Genome browser session (e.g. UCSC)	*Provide a link to an anonymized genome browser session for "Initial submission" and "Revised version" documents only, to enable peer review. Write "no longer applicable" for "Final submission" documents.*

Methodology

Replicates	*Describe the experimental replicates, specifying number, type and replicate agreement.*
Sequencing depth	*Describe the sequencing depth for each experiment, providing the total number of reads, uniquely mapped reads, length of reads and whether they were paired- or single-end.*
Antibodies	*Describe the antibodies used for the ChIP-seq experiments; as applicable, provide supplier name, catalog number, clone name, and lot number.*
Peak calling parameters	*Specify the command line program and parameters used for read mapping and peak calling, including the ChIP, control and index files used.*
Data quality	*Describe the methods used to ensure data quality in full detail, including how many peaks are at FDR 5% and above 5-fold enrichment.*
Software	*Describe the software used to collect and analyze the ChIP-seq data. For custom code that has been deposited into a community repository, provide accession details.*

Flow Cytometry

Plots

Confirm that:

☐ The axis labels state the marker and fluorochrome used (e.g. CD4-FITC).

☒ The axis scales are clearly visible. Include numbers along axes only for bottom left plot of group (a 'group' is an analysis of identical markers).

☒ All plots are contour plots with outliers or pseudocolor plots.

☒ A numerical value for number of cells or percentage (with statistics) is provided.

Methodology

Sample preparation	BM-cDC1 sort: Single cell suspensions from murine bone marrow were cultured with FLT3L to generate bone-marrow-derived DCs after red blood cells depletions. Following 8 days of culture at 37oC, cells were stained for 30 min on ice in order to sort BM-cDC1. BD Cytometric Bead Array measurement: performed on supernatant collected from stimulated BM-cDC1s PhosFlow: performed on stimulated BM-DCs subjected to 10min incubation at 37oC with warm PhosFlow Lyse/Fix Buffer, followed with resuspension in PhosFlow Perm Buffer III and incubation for 30min on ice. Samples washed twice and stained for an hour at room temperature. Intracellular staining: 10 days after infection, splenic HSV-1 gB498-505-specific CD8+ T cells were peptide restimulated for 5 h ex vivo. Single cell suspensions were stained with antibodies targeting surface markers and upon fixing and permeabilization with BD Cytofix/Cytoperm stained for 20 min at room temperature with intracellular IFNg-targeting antibody in BD Perm/Wash buffer.
Instrument	BM-cDC1 sort: FACS Aria III (BD Biosciences). BD Cytometric Bead Array and intracellular staining measurements: LSR Fortessa (BD Biosciences) PhosFlow: Cytek Aurora
Software	FlowJo software (v10.7.1)
Cell population abundance	BM-cDC1 sort: cDC1 represent 30 to 40% of living cells in FLT3L in vitro cultures. Purity check was systematically performed following each individual sort.
Gating strategy	BM-cDC1 sort: Cell population was first gated on FSC-A vs SSC-A and doublets were further excluded through FSC-H vs FSC-W followed by SSC-H vs SSC-W. Dead cells were excluded via propidium iodide (PI) staining. BM-cDC1 were identified by CD24 high SIRPa low CD11b low and CD45R/B220-. Flow Cytometry following HSV infection and restimulation: Lymphocytes were first gated on FSC-A vs SSC-A and doublets were further excluded through FSC-H vs FSC-W followed by SSC-H vs SSC-W. Dead cells were excluded (near IR). Next, CXCR6-/- CD8+ T cells were gated on CD45.2+, CD8+, CD44+, while WT CD8+ T cells were gated on CD45.1+CD45.2+ CD8+, CD44+ when respectively applicable.. The IFN-g+ cells were subjected to measurement. In the case of bone marrow chimera, CD45.1+ original recipient cells could be identified as CD45.1+ and these were mostly replaced by the donor bone marrow.

☐ Tick this box to confirm that a figure exemplifying the gating strategy is provided in the Supplementary Information.